Intermolecular interactions in cluster anions

Andrei Sanov *

Department of Chemistry and Biochemistry, The University of Arizona, Tucson, AZ 85721, U.S.A.

* Email, sanov@arizona.edu

We present a broad-brush picture of the covalent and electrostatic interactions controlling the structures and stabilities of cluster anions and discuss how one should think about chemical bonding in these species. Accordingly, the review emphasises the broad general trends, which stem from the aggregate nature of clusters rather than from the individual chemistry of the compounds comprising the specific systems considered. The offered perspective relies on a coupled-monomers approach, which assumes first-order separability of the inter- and intra-monomer interactions. It effectively treats the cluster components as interlocking but self-contained building blocks. A Hückel-style formalism, adapted specifically to a mixed network of covalent and solvation interactions in cluster anions, offers general insight into the cooperation and competition between the multitudes of interactions implicated in solvated environments.

Keywords: Cluster anions; Solvation; Covalent interactions; Photoelectron spectroscopy.

Table of Contents

1. Introduction 3

2. A brief classification of cluster anions 6

3. Covalent interactions and charge-sharing 8

3.1. Basic types of covalent dimer anions
3.2. The MO perspective
3.2.1. Type I: Dimer anions of closed-shell molecules
3.2.2. Generalisation and limitations of the coupled-monomers model
3.2.3. Type II: Dimer anions of radicals and diradicals
3.2.4. Type III: Charge-sharing dimerisation via singlet-triplet excitation of the monomers

4. Hückel-style treatment of cluster anions of closed-shell monomers 21

4.1. Ion-molecule solvation interactions
4.2. Charge-sharing polymerisation
4.2.1. Covalent dimer anions of closed-shell molecules
4.2.2. Covalent trimer anions of closed-shell molecules
4.2.3. Anionic tetramers (and beyond) of closed-shell molecules
4.2.4. Anionic arrays of different shapes and sizes
4.2.5. Generalisation of the charge-sharing trends

5. General factors controlling type-I cluster anion structures 36

5.1. Geometric constraints on covalent bonding
5.2. Effects of solvation on covalent bonding
5.3. Solvation hinders type-I polymerisation
5.4. Mixed-character interactions

6. Conclusion 44

Acknowledgements 45

REFERENCES 45

1. Introduction

Interactions between atoms and molecules are foundational to our world. In a hypothetical universe without such interactions, there would be no condensed matter, no life, and sadly no chemists to write or read texts like this, for the very subject of chemistry would not exist there.

Back in the real world, the importance of intermolecular forces was first postulated 150 years ago by none other than van der Waals, after whom some of such interactions are named today. Since then, scientists have developed many elegant ways of studying the intermolecular interactions and their effects on the properties of materials. Understanding chemical matter starts with uncovering the molecular-level details of the forces involved. If one were to design an optimal method from scratch, they would certainly want to bring the microscopic action of specific interparticle interactions to the foreground, while minimising the background from the overwhelming multitude of interactions in a bulk system. And that is where clusters come in.

Clusters (as known in chemistry) are ideal for studying pairwise and many-body intermolecular interactions [1,2]. Their structures and stability are controlled by these forces, and yet, unlike the bulk environments, they are small enough for the individual interactions to be resolved without excessive averaging. It is for these reasons that chemists often view clusters as unique microscopic laboratories perfectly suited for dissecting the bonding glue that holds our world together [3-5]. The modern field of cluster science is so vast, it allows for some miscellany of definitions of what constitutes a cluster. In this review, we view clusters as aggregate species composed of interacting, yet largely self-contained atomic or molecular moieties. Even in clusters of increasing size, these moieties preserve their individual identities and *intra*molecular bonding properties. They are bound together by *inter*molecular (or *inter*atomic) interactions, which are predominantly noncovalent or weakly-covalent in character.

We will focus only on ionic, specifically *anionic* clusters. Compared to their neutral counterparts, cluster anions stand out in many respects. Their excess charge results in an increased

Uncommon acronyms used in this paper

MMO MonoMer Orbital (molecular or atomic, depending on the nature of the monomer). Used here to delineate between the orbitals of one monomer and those of the cluster. Symbol ψ is used for the MMOs throughout.

LVO Lowest-Vacancy Orbital. The lowest-energy MMO with at least one vacancy. The LVO of a specific monomer $X^{(i)}$ is denoted $\psi_{\mathrm{LVO}}^{(i)}$.

IM InterMonomer (intermolecular or interatomic, depending on the monomers).

IMO InterMonomer Orbital. A cluster orbital defined as a linear combination of the MMOs of two or more monomers. Symbol ϕ is used for the IMOs throughout.

CMMO Coupled-Monomers MO model.

CSE Cluster Stabilization Energy. The overall stabilization energy of X_n^- relative to the $X^- + (n-1)X$ limit. Defined as a positive value and includes both covalent and electrostatic (solvation) interactions within the cluster.

VSE Vertical Stabilization Energy, the vertical counterpart of CSE, excluding the monomer relaxation energy upon cluster dissociation. Defined as the overall stabilization energy of X_n^- relative to the non-interacting $X^- + (n-1)X$ ensemble, where the energies of both X^- and X are determined at the geometry of these moieties within the cluster. CSE = VSE $- \Delta E_{\mathrm{rel}}$, where ΔE_{rel} is the combined relaxation energy of all monomers.

strength of the noncovalent forces, as the ion-neutral interactions are generally stronger than the van der Waals attraction between neutral atoms or molecules. With that in mind, the cumulative effect of noncovalent interactions in cluster anions, commonly referred to as anion solvation, may easily compete with covalent bonding [5]. On the other hand, coherent charge sharing may lead to new covalent bonds between the cluster building blocks. Overall, to understand the properties of cluster anions, one must consider the interplay between the two types of forces, as well as the mechanism of binding and distribution of the excess charge.

The objective of this review is to give a broad-brush, bird's eye perspective of the interplay between covalent bonding and solvation in cluster anions. This is not an exhaustive appraisal of the field, but a focused reflection on the recent developments that directly impact the above objective. We will forego extensive discussion of specific measurements or systems, in favour of an elementary description of the general trends in size-dependent cluster structures.

On a pairwise basis, the noncovalent (electrostatic) interactions implicated in anion solvation are generally weaker than the chemical bonds in either the solute or the solvent. For this reason, the very idea of competition between the two types of forces (one being generally weak, the other generally strong) may seem implausible. However, in a large enough cluster, the combined effect of the solute interactions with all solvent species, including the many-body effects [6], can exceed the energy of a covalent bond, especially if the bond in question is weak. This sets up a thermodynamic mechanism for effective competition between covalent bonding and solvation, capable of hindering the formation of dimer or polymer anions in solvated environments. In short, even in systems prone to covalent bonding, the formation of dimer or polymer anions is not assured, as it may be hindered by the solvent, if it becomes energetically favourable to sacrifice covalent bonds in favour of maximising the noncovalent interactions.

In particular, it has been long understood that electrostatic interactions within the first solvation shell favour smaller core-anion sizes [5]. For example, in the monomer- vs. dimer-anion based cluster series, the monomer anions interact stronger with the nearest solvent molecules than the dimers, due to their smaller size and more localised charge. It is for this reason that solvation interactions often tilt the scale in favour of the monomer-based cluster structures, compared to the dimer- or polymer-based counterparts.

The $(CO_2)_n^-$ cluster series is a classic example of this behaviour. In the $n = 2–5$ size range, these clusters famously have the covalent dimer-anion cores, $(CO_2)_2^-$ [7,8], with a relatively weak bond connecting the two CO_2 moieties, as initially proposed in 1987 by Fleischman and Jordan [9]. In these relatively small clusters, the significant stabilisation from the new covalent bond favours the $(CO_2)_2^-(CO_2)_{n-2}$ cluster structures. However, already for $n = 6$, the monomer-based species, $CO_2^-(CO_2)_5$, have been observed to coexist with the dimer-based clusters, $(CO_2)_2^-(CO_2)_4$ [7,8,10-12]. This implies that in $(CO_2)_6^-$ the effect of the additional order-of-1/2 covalent bond in the dimer anion plus this anion's solvation by the remaining four CO_2 molecules is approximately the same as that of CO_2^- solvation by five neutral molecules. Simply put, in the presence of a few solvent molecules, it is energetically favourable to form the dimer anion, but the interaction of this bulkier ion with each of the solvent molecules is weaker than that of the more compact CO_2^- with the same CO_2 molecules. We will call this effect the solvation differential. The more CO_2s are added to the clusters, the larger the differential, i.e., the price of keeping the dimer anion intact. In $(CO_2)_6^-$ and larger clusters, it becomes preferable to yield to the solvation rather than form or maintain a covalent bond between the monomers.

The competition between covalent bonding and solvation can be elucidated by photoelectron spectroscopy [13]. While solvated anions are stabilized by ion-neutral interactions, the corresponding neutral states are affected to a lesser degree, because of the relative weakness of the van der Waals forces. Therefore, as the cluster size increases, solvation results in discernible shifts of the photodetachment transitions towards larger electron binding energies (eBE) [3,5]. In the absence of chemical rearrangements, the increase in eBE with the cluster size is usually gradual and monotonic. Discontinuities in this trend signal abrupt changes in the electron binding and the structure of the cluster core [7,8,14-31].

In the specific case of $(CO_2)_n^-$, the photoelectron spectra of these size-selected clusters display two different band series: one, corresponding to higher vertical detachment energies (VDE), is observed for n = 2–6 and $n \geq 14$; the other, with lower VDEs, is observed in the n = 6-13 range [7,8]. The discontinuities at n = 6 and 14, which cannot be accounted for by solvation, are attributed to structural changes in the cluster core. These changes have been termed core-switching. The "switch" is from the covalently bound dimer anion to the CO_2^- monomer, occurring at n = 6 [7,8]. A reverse switch, back to the dimer, is observed at n = 14, corresponding to the completion of the first solvation shell in $(CO_2)_2^-(CO_2)_{12}$.

Tsukuda et al. discovered a similar phenomenon in $(NO)_n^-$ [32]. For this series, the VDE increases by more than 2 eV from n = 1 to n = 2 and by nearly 1 eV from n = 2 to n = 3. Much smaller consecutive increases (~0.1–0.2 eV each) are observed in the n = 3–7 range. While the n = 3–7 trend is consistent with stepwise solvation, the abrupt jumps between n = 1 and 2 and between n = 2 and 3 signal structural changes in the core anion. The n = 1 species is unambiguously NO^-, but n = 2 was shown to be a covalently bound dimer anion, $(NO)_2^-$ or $N_2O_2^-$, for which several isomeric forms have been proposed [29,33-38]. The n = 3 cluster is (predominantly) a covalent trimer, $(NO)_3^-$. Summarising these findings, in the n = 1–3 range the excess electron in $(NO)_n^-$ is shared between all available NO moieties, but in larger clusters the size of the core anion no longer increases with n [32].

This behaviour is observed in many cluster systems. A central question in this review is why electron binding is so often limited to just 1-3 cluster building blocks. Sometimes, the key lies in the reaction dynamics and cluster formation mechanism, but at thermal equilibrium it comes down to the relative stabilities and free energies of the clusters with different core types. We consider the underlying trends by focusing on the electronic-structural factors that promote or hinder anionic bond formation and control the relative stabilities of cluster isomers.

As a practical approach, we will consider the interactions between cluster building blocks within the general framework of a coupled-monomers model. As the name implies, our broad approach assumes that the building blocks of a cluster (the monomers) largely preserve their identities and internal bonding structures. The interactions (couplings) between the monomers can therefore be considered separately. Both covalent and electrostatic (solvation) forces are included as the inter-monomer (IM) coupling vehicles. Under the above assumption, both types of interactions can be treated, effectively, as perturbations, This is justified only if the IM forces are weak or can be decoupled from the intra-monomer structures for other reasons. This approach works remarkably well for analysing the bonding power of a single electron added to a network of closed-shell monomers—a general problem to which this text devotes considerable discussion. Since the general molecular-orbital (MO) theory is the logical foundation for the description of covalent interactions [39], the overall formalism overviewed here is referred to as the coupled-monomers molecular-orbital (CMMO) model [40].

In Section 2, we set the stage and define some of the necessary terminology by giving a brief classification of the species known as cluster anions. Section 3 gives a qualitative description of IM covalent bonding rooted in the general MO theory. Section 4 details a quantitative treatment of both covalent and electrostatic IM interactions and devotes considerable discussion to the fundamental limits of the bonding power of an electron added to an network of closed-shell monomers. Sections 5 combines the mathematical treatment of both types of couplings from Section 4 into a unified model, yielding specific conclusions about the general trends in cluster structures.

This text uses several uncommon acronyms. To help the reader follow any part without having to search for the previously made definitions, they are summarised in the inset on the first page of the Introduction.

2. A brief classification of cluster anions

To clearly define some of the terminology used throughout, this section gives a broad, but not exhaustive, classification of the species known as cluster anions [40], drilling down only on the specific types discussed in this work. As shown in Figure 1, cluster anions are divided into the homogeneous (a-c) and heterogeneous (d) types. Like "cluster", these terms have many possible meanings. As used here, they apply only to the chemical identities of the cluster building blocks, the monomers. A homogeneous cluster anion consists of n identical molecular or atomic monomers X, which bind an excess electron in some fashion. Well-known examples include $(H_2O)_n^-$, $(CO_2)_n^-$, Ar_n^-, and O_{2n}^-. All these cluster families can be described by the generic molecular formula X_n^-, with X = H_2O, CO_2, Ar, and O_2, respectively. In contrast, a heterogeneous cluster consists of at least two types of monomers, such as $Br^-{\cdot}Ar_n$, $I_2^-(CO_2)_n$, $(CO_2)_n^-(H_2O)_k$, and others.

Molecular formulas do not convey structural information, nor do they provide full indication of how the excess charge is bound to the cluster. In the ground state of a heterogeneous cluster anion, the excess electron naturally binds to a moiety or moieties with greater electron

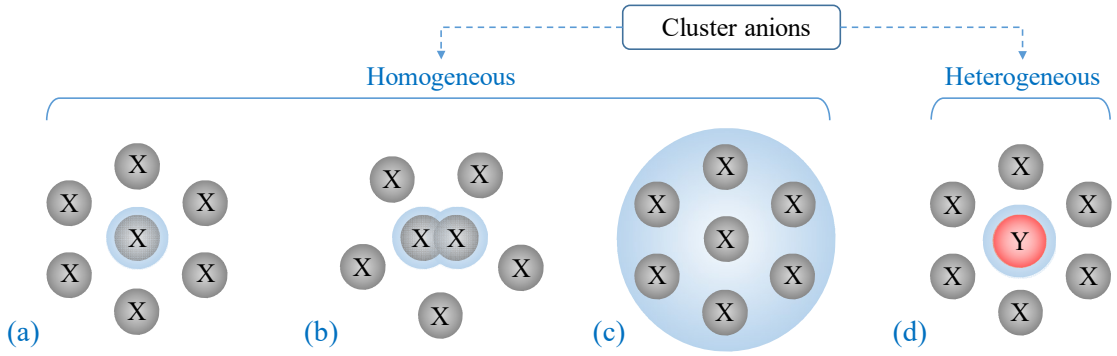

Figure 1. Classification of cluster anions used in this review. The grey and red spheres represent atomic or molecular monomer of arbitrary types X and Y. The blue halos represent the diffuse wave function of the excess electron. (a)-(c) Homogeneous X_n^- cluster anions. The sketch in (a) is a schematic representation of a monomer-based cluster, $X^-{\cdot}X_{n-1}$. (b) Cluster anions with the excess charge shared among a subset of the monomer building blocks, $X_k^-{\cdot}X_{n-k}$, $2 \le k \le n$. The specific sketch shown corresponds to $k = 2$ (a covalently bound dimer-anion cluster core). (c) Clusters with an excess electron not bound in valence orbitals of the monomers, localized instead in a solvent cavity or delocalized over the surface or the bulk of the cluster. (d) An example of a valence heterogeneous cluster anion, $Y^-{\cdot}X_n$.

affinity. This often results in a well-defined, clearly-localised charge distribution, as in $Br^-{\cdot}Ar_n$ and $I_2^-(CO_2)_n$. Both are examples of a generic $Y^-{\cdot}X_n$ cluster anion, with Y = Br or I_2 and X = Ar or CO_2. This case is illustrated in Figure 1(d), where the grey and red spheres represent atomic or molecular monomer moieties of types X and Y, respectively, while the blue halo around Y represents the diffuse wave function of the excess electron, bound specifically to this monomer. In a $Y_n^-{\cdot}X_k$ cluster, e.g., $(CO_2)_n^-(H_2O)_k$, possible charge sharing between equivalent Y monomers may complicate this simple picture.

This work focusses primarily on homogeneous clusters, X_n^-. In them, all monomer units are nominally equivalent, creating a range of possibilities for the excess electron binding. As illustrated in Figure 1(a)-(c), the unit of negative charge in X_n^- can be localised on a single moiety X, shared between the valence orbitals of several monomers, or delocalised over the entire cluster. To describe the different electron binding motifs, we will often turn to the more informative, structural variants of the generic formula X_n^-. The first possibility, illustrated in Figure 1(a), has the charge (represented by the blue halo) localized on a single monomer, as conveyed by the structural formula $X^-{\cdot}X_{n-1}$. The anionic moiety X^- in this case is the cluster core, while the remaining $(n - 1)$ neutral monomers are solvents, bound to the core anion (the solute) by noncovalent interactions. An example of $X^-{\cdot}X_{n-1}$ clusters can be found in the $(CO_2)_n^-$ series: in the n = 7–13 range, these clusters have CO_2^- cores [7,8].

Alternatively, the charge in X_n^- may be shared among a subset of the monomers, as conveyed by the structural formula $X_k^-{\cdot}X_{n-k}$, $2 \le k \le n$. In this case, X_k^- is the cluster core, solvated by $(n - k)$ neutral solvent moieties. Clusters of this kind often have dimer-anion cores (k = 2), with the core anion consisting of two monomers, which share the excess electron. For example, this is the case in the $(CO_2)_n^-$ series, with $2 \le n < 6$ and $n \ge 14$ [7,8]. A generic illustration of a homogeneous dimer-based cluster anion is shown in Figure 1(b). The shared electron in this case (the blue halo) occupies a molecular (cluster) orbital, which is shared between the two X moieties. This cluster orbital can be described as a superposition of the valence orbitals of two monomers, and we will generally refer to such orbitals as inter-monomer orbitals, IMO. It is important to stress that such electron sharing is coherent in nature. As in the general MO theory, population of a bonding IMO by an electron contributes to the inter-monomer covalent bonding and leads to the formation of a covalently bound X_2^- dimer anion, the core of the $X_2^-{\cdot}X_{n-2}$ cluster. Clusters with trimer-anion (k = 3) or even larger cluster cores are also conceivable, and some possible examples are discussed in the following sections of this review.

In the third type of homogeneous cluster anions is illustrated in Figure 1(c). Here, the excess electron is not bound to the valence orbitals of any specific monomer or monomer group. Instead, it can be localized in a solvent cavity or delocalized over the surface or the bulk of the cluster. Perhaps the most famous example of such species are the hydrated-electron clusters, $(H_2O)_n^-$ [41-54]. To be clear, clusters of this type do not correspond to the $k = n$ limit of the $X_k^-{\cdot}X_{n-k}$ case described above. The excess electron in Figure 1(c) does not enter the valence orbitals of the monomers and, therefore, does not create IM covalent bonds. This scenario occurs when the lowest valence orbital of X with a vacancy in it lies too high in energy to enable the formation of a valence X^- or X_k^- anion. In such a cluster, there is no core anion, unless one considers the electron itself as the cluster core.

In the rest of this work, we focus on homogenous valence cluster anions of the types illustrated in Figure 1(a) and (b). They can be described collectively as $X_k^-{\cdot}X_{n-k}$, $1 \le k \le n$. The

crucial element defining the properties of these species is the cluster core structure. Given the possibility of forming dimer or polymer anions in cluster environments, the core structures are subject to the competition between IM covalent bonding and electrostatic solvation. Among the covalent X_k^-, $k \geq 2$ core ions themselves, it is important to further distinguish between the dimer or polymer species formed from closed-shell monomers and those formed from radicals or diradicals. This distinction plays a defining role in not only the geometric, but also the electronic structure of the cluster core.

With closed-shell monomers, the IM covalent bonding in X_k^- is usually a consequence of electron attachment. In the absence of an additional electron, most closed-shell neutral monomers interact with each via weak van der Waals forces. Upon electron attachment, the new IM bond(s) may form due to the added electron entering the IMO system, which emerges in the dimerisation or polymerisation process. The reverse process (i.e., the lowest-energy electron detachment transition) would cause X_k^- to fall apart to k unbound (or weakly interacting) X moieties: $X_k^- \rightarrow k\,X + e^-$ (dissociative detachment) [55,56].

Such phenomena rely on coherent charge-sharing for the IM bonds to form and are, therefore, logically referred to as *anionic charge-sharing dimerisation* or (when appropriate) *polymerisation* [40]. Despite some similarity in the terms, they should be clearly distinguished from *anionic addition* (chain-growth) polymerisation, which is initiated by anions and involves the propagation of a *localised* negative charge [57]. Perhaps the best known example of charge-sharing dimerisation is the already mentioned $(CO_2)_2^-$ dimer [9], the core of the $(CO_2)_n^-$ clusters with $2 \leq n \leq 6$ and $n \geq 14$ [7,8]. In this dimer, the two CO_2 moieties are bonded by an order-of-1/2 IM covalent bond, which is due exclusively to the excess electron populating a bonding superposition of the two CO_2's lowest-unoccupied molecular orbitals.

With the radical or diradical building blocks, the X_k^- anions can often (but not always) form by electron attachment to stable X_k molecules. Essentially, the high reactivity of radicals and diradicals leads to their easy dimerisation or, sometimes, polymerisation in the neutral state. One simple example of this is F_2^-, which can be nominally viewed as a product of neutral-state dimerisation of two F· radicals, with an extra electron added to the resulting F_2 dimer. Since the anionic charge is not responsible for the formation of the dimerising bond (it actually weakens it), the formation of this anion should not be described as anionic charge-sharing dimerisation, per se, even though charge sharing does occur. Most of the rest of this review is devoted to the cluster anions formed from closed-shell monomers, but to define the field a qualitative discussion of the radical- and diradical-based species is also included in Section 3.

3. Covalent interactions and charge-sharing

We start by considering covalent dimer anions. In theory, the results can be easily extended to trimers and beyond. In practice, it rarely happens. Sections 4 and 5 will discuss why.

3.1. *Basic types of covalent dimer anions*

In many known cases, the addition of an electron to a neutral X_n cluster leads to coherent charge-sharing and sometimes the formation of new covalent bonds between two or more monomers [7-12,15-29,33-38,40,58-64]. We begin with the simplest case, the homogeneous dimer anions X_2^-, in which the charge is coherently shared between two equivalent monomers. Three possible electronic motifs distinguishing these species can be readily identified [40]:

(I) Dimer anions formed via charge-sharing dimerisation of closed-shell monomers.
(II) Dimer anions of radicals or diradicals.
(III) A combination of I and II: Dimer anions formed from closed-shell molecules via an charge-sharing dimerisation process, which effectively involves a singlet-triplet excitation of the monomers.

The IM covalent bonding in each case can be understood by considering the overlap of the monomer orbitals, leading to the formation of the bonding and antibonding IMO pairs, the same way as linear combinations of atomic orbitals (AO) yield molecular orbitals within the LCAO-MO theory framework. To delineate between the molecular orbitals that describe the entire cluster or the cluster core (i.e. the IMOs) from the orbitals that belong to a single monomer, the acronym MMO (for MonoMer Orbitals) is used to describe the individual monomers. Depending on the nature of X, an MMO can be either a molecular or atomic orbital (in the cases of molecular and atomic monomers, respectively). In the coupled-monomers MO model (CMMO), the IMOs are represented by linear combinations of the MMOs of different monomers. That is, the MMOs and IMOs in the CMMO model play the same respective roles, as the AOs and MOs in the LCAO-MO theory.

The key feature of type-I dimerisation is that the IM bond in X_2^- forms due to the excess electron populating a bonding IMO. For example, there is no covalent bonding between the two CO_2 moieties in the $(CO_2)_2$ van der Waals dimer, but in $(CO_2)_2^-$ [9] the excess electron enters an IMO described as a bonding superposition of the lowest-unoccupied orbitals of the two monomers [22]. The resulting electron configuration yields an order-of-1/2 IM bond, which is typical of type-I dimer anions. More on this in Section 3.2.1.

Type-II dimers involve the anionic pairing of neutral radicals or diradicals. Contrary to type-I cases, the IM bonding in type-II dimers is not necessarily due to the excess electron. Radicals and diradicals often dimerise in the neutral state. For this reason, many (but not all—see Section 3.2.3) type-II dimer anions are best thought of as products of electron capture by neutral dimer molecules. For example, F_2^- is (technically) a type-II dimer anion of atomic fluorine. Because of the pre-existing neutral bonds, one usually does not think about type-II anions as products of *anionic* dimerisation, because no charge is required for the dimerisation to occurs. However, in some cases, such as O_4^- [58-63], the IM bond formation indeed occurs in the anion state. More on this in Section 3.2.3.

Finally, type-III dimerisation pairs monomers, which are closed-shell singlets in their ground states but yield dimer anions whose neutral core configurations are best described in terms of singlet coupling of the monomers promoted to their respective triplet states. That is, one can say that the neutral dimer electron configuration, obtained via the lowest-energy photodetachment transition in the dimer anion, is doubly excited [16,25]. This is not meant to imply that for type-III dimer anions to form, the neutral monomers must first undergo singlet-triplet excitations. The more straightforward pathway usually involves the anionic dimerisation of singlet monomers (a type-I process), followed by internal conversion to the doubly excited (and yet, more favourable) configurations in the anion state. Regardless of the mechanistic details, the language of double excitations is valuable, because it provides a clear depiction of the electronic structures of these species. More on type-III dimers in Section 3.2.4.

3.2. *The MO perspective*

3.2.1. Type I: Dimer anions of closed-shell molecules

We begin the discussion of the molecular-orbital mechanics of covalent interactions by considering homogeneous dimer anions X_2^-, in which the excess electron is shared equally and coherently between the equivalent monomers. The dimer-anion of carbon dioxide, $(CO_2)_2^-$ [7,8,22,65], is an already-mentioned example of such species. We will continue using it for illustration purposes, but the same conceptual formalism can be readily applied to numerous other systems, including the π stacked dimer-anions and dimer-cations of various organics [39,40,66-68]. These dimers are the simplest cases of anionic (or cationic) bonding between monomers that are closed-shell species in their respective neutral states.

The IM covalent bond in such dimer anions results from the electron capture by a cluster orbital (IMO) described as a bonding superposition of the lowest-unoccupied orbitals of the neutral monomers. Hence, we start the description of these species from defining the active orbitals of the monomers. In general, assume that two neutral closed-shell monomers X, identified as $X^{(1)}$ and $X^{(2)}$, each have an electron configuration:

$$X^{(i)}\text{: } \ldots (\psi^{(i)}_{\mathrm{LVO}-1})^2 (\psi^{(i)}_{\mathrm{LVO}})^0 \tag{1}$$

Here, $\psi^{(i)}_{\mathrm{LVO}}$ is the lowest-vacancy orbital (LVO) of $X^{(i)}$, i = 1, 2, and $\psi^{(i)}_{\mathrm{LVO}-1}$ is the MMO just below it in energy. The uncommon term LVO is introduced to avoid the ambiguity associated with the commonly used terms HOMO and LUMO in the diverse cases of closed-shell, radical, diradical, and anion systems. Our focus is on the ground states of anions, which are generally obtained by adding an electron to the lowest available *vacancy*, not necessarily the lowest completely unoccupied orbital of the neutral. That is, the key to anion formation is not necessarily the LUMO, but the lowest-energy orbital with at least one vacancy in it, the LVO. The LUMO assumes the role of the LVO for closed-shell species. For radicals, however, the LVO is the singly-occupied HOMO, while for diradicals it is either the HOMO or HOMO−1, depending on the HOMO degeneracy and the state multiplicity.

For reference, the electron configuration of the valence monomer anion is described as:

$$(X^{(i)})^-\text{: } \ldots (\psi^{(i)}_{\mathrm{LVO}-1})^2 (\psi^{(i)}_{\mathrm{LVO}})^1 \tag{2}$$

Using this nomenclature, Figure 2 illustrates the general case of anionic charge-sharing dimerisation of closed-shell monomers, with the LVO and LVO−1 sketches corresponding to the case of X = CO_2. The overlap of the respective MMOs of the $X^{(1)}$ and $X^{(2)}$ moieties yields pairs of bonding and antibonding IMOs, defined as:

$$\phi^{(\pm)}_{\mathrm{LVO}} = \psi^{(1)}_{\mathrm{LVO}} \pm \psi^{(2)}_{\mathrm{LVO}} \tag{3}$$

$$\phi^{(\pm)}_{\mathrm{LVO}-1} = \psi^{(1)}_{\mathrm{LVO}-1} \pm \psi^{(2)}_{\mathrm{LVO}-1}$$

$$\ldots$$

The normalization factors are omitted in these equations. With ψ reserved for the monomer orbitals, ϕ is used to denote the IMOs. The subscripts for each IMO indicate the orbital's genesis: for example, $\phi^{(\pm)}_{\mathrm{LVO}}$ are formed by the overlap of the LVOs of the two monomers.

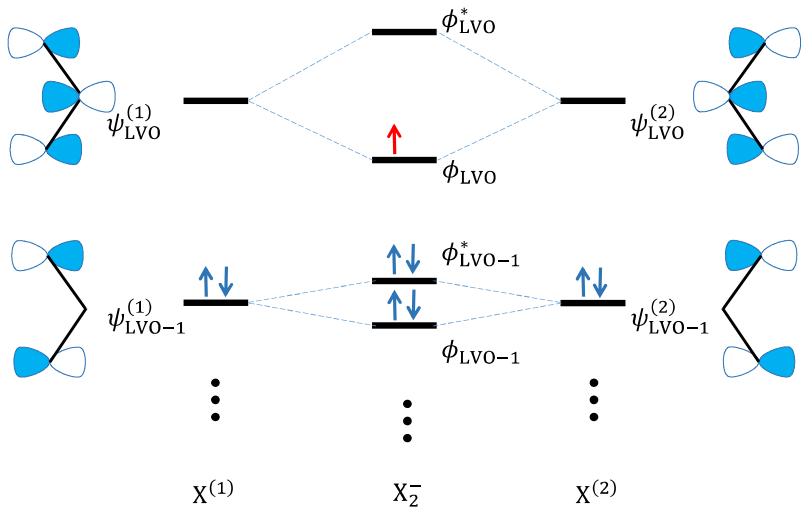

Figure 2. Generic IMO diagram for type-I anionic dimerisation. The MMO sketches correspond to X = CO_2 (or similar molecules) at a bent anion geometry. See the text for details.

The ± sign in Equation (3) describes the formation of the bonding or antibonding IMO pairs. As in the LCAO-MO theory, the IMO bonding character depends not only on the sign of the superposition, but also the symmetry of the MMOs with respect to each other. In Figure 2, $\phi^{(+)}_{\mathrm{LVO}}$ and $\phi^{(+)}_{\mathrm{LVO}}$ are the bonding IMOs, but in other scenarios the plus signs can result in antibonding superpositions. To avoid this ambiguity, we replace the ± notation with the conventional asterisk sign and the lack thereof to denote the antibonding and bonding IMOs, respectively. With that, the electron configuration of the covalently bound dimer anion, based on the IMO diagram in Figure 2, is written as:

$$X_2^-\text{: } \ldots (\phi_{\mathrm{LVO-1}})^2(\phi^*_{\mathrm{LVO-1}})^2(\phi_{\mathrm{LVO}})^1 \tag{4}$$

This configuration corresponds to a nominal IM bond order of 1/2 and a –0.50/–0.50 charge sharing between the two monomers. The dimerising bond is entirely due to the excess electron (red arrow in Figure 2) populating ϕ_{LVO}. The bond disappears (its order is reduced to zero) if the electron is removed.

This analysis builds on other variants [69,70] of the general MO theory. Particularly noteworthy, Krylov and co-authors used a similar approach (adapted to electron removal rather than addition) to investigate the bonding patterns in dimer cations of benzene [39], uracil [66], adenine and thymine [67]. They fittingly named their theory dimer MO—linear combination of fragment MOs (DMO-LCFMO) [39]. It is only because the present work extends beyond the dimers that we use the more general term IMO instead of DMO.

While the MMO sketches in Figure 2 correspond to X = CO_2, the qualitative IMO energy diagram applies to other systems of closed-shell neutral monomers, as well. The specific case of anionic π-stacking of glyoxal, biacetyl, and other similar organic molecules was recently discussed elsewhere [40]. For the sake of illustration, the bonding IMO (ϕ_{LVO}) for the biacetyl (ba) dimer anion is shown in Figure 3(b), where it can be compared to the monomer LVO ($\psi^{(1)}_{\mathrm{LVO}}$) shown in Figure 3(a). The dimer IMO shown can be described as a superposition of the

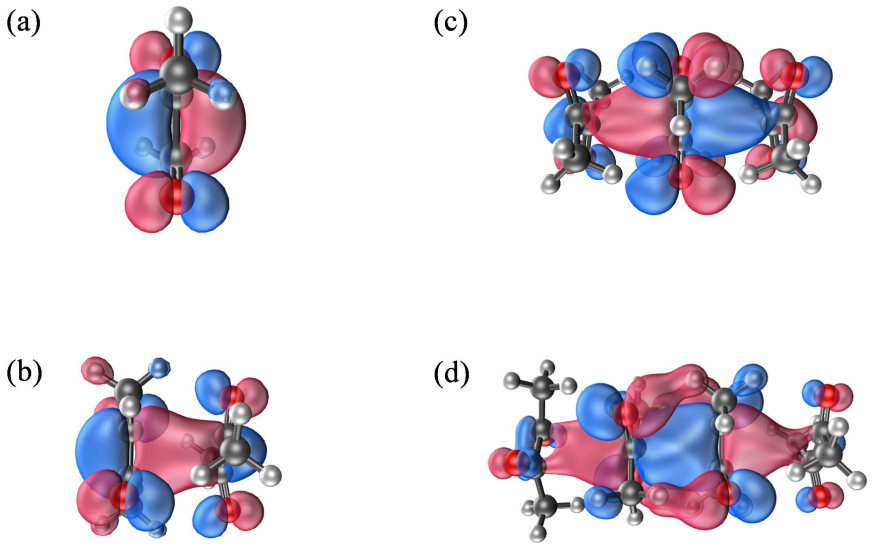

Figure 3. The orbitals populated by radical electrons in the equilibrium structures of (a) ba^-, (b) $(ba)_2^-$, (c) $(ba)_3^-$, and (d) $(ba)_4^-$, where ba = biacetyl.

LVOs of the two monomers, $\psi_{\mathrm{LVO}}^{(i)}$, i = 1, 2: envision combining the MMO in Figure 3(a) with its reflection in a plane to the right of the molecule, rotated about the IM (horizontal) axis by some degree, and the result is a close approximation to the dimer IMO in (b). Granted, a slight deviation from the even density distribution in the dimer is revealed by close comparison of the two moieties in Figure 3(b). It seems to contradict the expectations based on Equation (3), but this is partially a visual artefact (due to the different orientations of the two monomers in the dimer with respect to the viewing axis) and partially the result of the two ba moieties in the dimer anion indeed being not exactly equivalent. That non-equivalence is due to different methyl group orientations, as discussed in Ref. [68]. This structural intricacy is important for the properties of $(ba)_2^-$ specifically, but not important for the present discussion.

3.2.2. Generalisation and limitations of the coupled-monomers model

Subject to certain geometry limitations (discussed in Section 5.1), the dimer formalism from Section 3.2.1 is easily extended to the trimer, tetramer, and larger polymer anions. Regardless of the size of the polymer anion chain, the type-I IM bonding is due to a single excess electron entering the IMO system of the otherwise non-interacting neutral closed-shell monomers.

In the MO theory, one bonding electron yields a bond order of 1/2, and that is the nominal bond order in the type-I X_2^- dimer anion, represented by the IMO diagram in Figure 2. In larger systems, i.e. X_n^-, $n \geq 3$, the one bonding electron, and the same corresponding order-of-1/2 bonding character are shared between multiple IM bonds. This phenomenon is reviewed in Sections 4.2 and 5.3, but for now note that in the $(ba)_n^-$ example illustrated in Figure 3, the singly occupied IMO is responsible for two IM bonds in the trimer (c) and three in the tetramer (d). Therefore, the Lewis-style order of each of the IM covalent bonds is progressively reduced from the dimer to the trimer and to the tetramer. In the stacked or chain $[X\text{-}X\text{-}X]^-$ trimer anion, the two X-X bonds are equivalent, and each is assigned a nominal order of 1/4. In the tetramer, $[X^{(1)}\text{-}X^{(2)}\text{-}X^{(3)}\text{-}X^{(4)}]^-$, the $X^{(1)}\text{-}X^{(2)}$ and $X^{(3)}\text{-}X^{(4)}$ bonds are equivalent, but $X^{(2)}\text{-}X^{(3)}$ is distinct, so the nominal assignment of a 1/6 bond order to each is an approximation.

As a straightforward generalisation of this picture, the larger the type-I polymer anion, the weaker the individual IM bonds holding it together [40]. With just one electron entering the lowest-energy IMO, the 1/2 bonding power is shared (being spread thin) among $(n-1)$ IM bonds. Neglecting the differences between the individual bonds depending on their placement, each bond order in a type-I X_n^- polymer-anion chain is $\frac{1}{2(n-1)}$, on average. It is not surprising, therefore, that the formation of long type-I chain anions is easily impeded by other interactions (e.g., solvation) or couplings (e.g., vibronic).

Before proceeding, a crucial limitation of the monomer-coupling model should be stressed. As presented, the model separates the IM bonding from the internal bonding structures of the monomers themselves. Such separation is formally justified only if the inter- and intra-monomer bonds are effectively decoupled. This approximation can be reasonably made, for example, in the case of the IMOs formed from nonbonding MMOs. The nonbonding MMOs, by definition, do not contribute to the intra-monomer bonding, but they can be combined with the corresponding orbitals of other monomers to result in intermonomer bonds.

On the other hand, if the monomer orbitals contributing to the IMOs are significantly involved in the intra-monomer bonding, the model amounts to a first-order approach, in which the IM bonding is treated as a perturbation of the intra-monomer bonding structures. The first-order approximation is justified only if the IM interactions are significantly weaker than the intra-monomer bonds. This requirement is often satisfied in dimer/polymer anions of closed-shell monomers, because of the weakness of the IM bonds in these systems. In systems with stronger IM bonds (e.g., radical or diradical monomers), strong IM bonding affects the electronic wavefunctions of the monomers, and, thus, the intra-monomer bonding properties. In that case, treating the IM bonding as a first-order perturbation of the intra-monomer bonds is no longer justified.

3.2.3. Type II: Dimer anions of radicals and diradicals

Type-II dimer anions involve the anionic pairing of neutral radicals or diradicals. In contrast to the type-I cases, the IM bonding in type-II dimers is not (always) dependent on the presence of an excess electron. Radicals and diradicals may readily pair up (dimerise) in the neutral state and many (but not all) type-II dimer anions are products of electron capture by neutral covalently bound dimers.

For example, F_2^- is (technically) a type-II dimer anion of atomic fluorine with an IM bond order of 1/2. Similarly, the anions of glyoxal (gl) [71] and fumaronitrile (fn) [64] may be classified as type-II dimer anions of the formyl radical (HCO) and cyanocarbene (HCCN), respectively [40]. Indeed, the neutral molecule of glyoxal, O(H)C–C(H)O, is a dimer of HCO, with an IM (C–C) bond order of 1. In the gl^- anion, this bond order increases to 1.5, because the glyoxal LUMO has a π bonding character with respect to this bond. On the other hand, when two HCCN moieties dimerise to form fumaronitrile, N≡C–C(H)=C(H)–C≡N, a double C=C bond is formed between the HCCN monomers, because cyanocarbene is a triplet-ground-state [72] diradical. In the fn^- anion, this bond is reduced to the nominal order of 1.5, because of the antibonding character of the fn LUMO with respect to the C=C bond.

We will limit the discussion of type-II dimer anions to the species consisting of monomers that are triplet-state diradicals in their ground states. However, the suggested formalism can be easily adapted to neutral radicals (doublets), as well. Triplet-ground-state diradicals have degenerate or near-degenerate orbitals populated by two unpaired electrons [73]. We refer to the

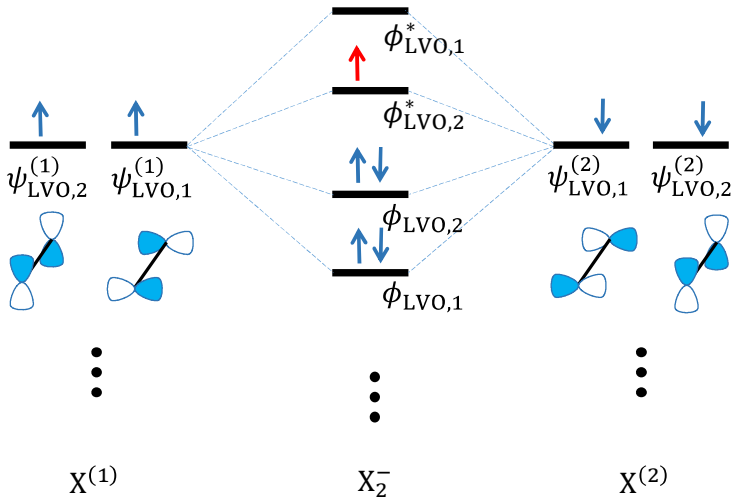

Figure 4. Generic IMO diagram for type-IIa anionic dimerisation. The MMO sketches correspond to X = O_2 (or similar molecules). See the text for details.

degenerate and near-degenerate cases as types IIa and IIb, respectively. The electron configuration of a neutral monomer in the general type-IIa case is:

$$\mathrm{X}^{(i)}(\text{Triplet}): \ldots(\psi^{(i)}_{\mathrm{LVO}})^2 = \ldots(\psi^{(i)}_{\mathrm{LVO},1})^1(\psi^{(i)}_{\mathrm{LVO},2})^1, \tag{5}$$

where i = 1, 2 is the same index as in Equations (1) and (2), while $\psi^{(i)}_{\mathrm{LVO},1}$ and $\psi^{(i)}_{\mathrm{LVO},2}$ are the degenerate LVOs (HOMOs) of $\mathrm{X}^{(i)}$, each populated by an unpaired electron. The corresponding monomer anions have the ground-state electron configuration:

$$(\mathrm{X}^{(i)})^-: \ldots(\psi^{(i)}_{\mathrm{LVO},1})^2(\psi^{(i)}_{\mathrm{LVO},2})^1 \tag{6}$$

The general type-IIa IMO diagram is presented in Figure 4. One particularly instructive specific case is the anionic dimerisation of O_2 to yield O_4^- [58-63]. Molecular oxygen in the ground electronic state is a triplet diradical, with two degenerate half-filled $\pi^*_g(2p)$ HOMOs, which have inspired by the MMO sketches in Figure 4. The diagram correctly predicts the qualitative properties of O_4^- [74,75]. Its rectangular (D_{2h} symmetry) structure [61] is shown in Figure 5(a), where it can be compared to the O_2 and O_2^- structures [63], shown in (b) and (c), respectively. Two of the O–O bonds in O_4^-, which we view as IM bonds, are weaker (longer)

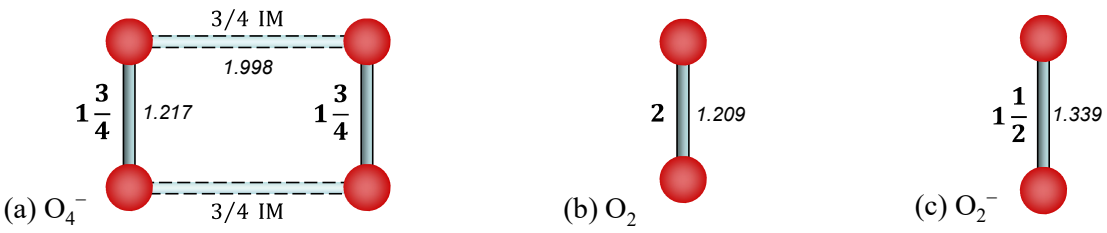

Figure 5. The equilibrium structures of (a) O_4^-, (b) O_2, and (c) O_2^-. The italicised values are the bond lengths in Angstroms. The integers and fractions in Roman type are the intra-monomer (bold) and intermonomer (plain) bond orders.

than the intra-monomer O–O bonds. Hence, as we did in the type-I case (Section 3.2.1), it is possible to separate approximately the IM bonding in the dimer from the intramolecular bonding within the two O_2 moieties and treat the former as a perturbation of the latter. The excess charge in O_4^- is equally shared between the two O_2 moieties and the O_4^- structure should be viewed as either $O_2^{-1/2}\cdots O_2^{-1/2}$ or $O_2^-\cdots O_2 \leftrightarrow O_2\cdots O_2^-$, where $\cdots$ indicates the charge-sharing IM interactions and $\leftrightarrow$ a resonance. The charge sharing is due to a coherent superposition of the monomer orbitals, yielding the O_4^- IMOs, as shown in Figure 4. These IMOs are populated by four bonding and one anti-bonding electrons, yielding a nominal IM bond order of 3/2. Since this bonding character is distributed among two equivalent O-O bonds, each of these IM bonds has an effective order of 3/4.

It is possible to correlate these bond orders with the corresponding bond energies by normalising the latter by the former. This exercise yields effective bond strength per unit bond-order. As we will see, the normalised strength of IM bonding in O_4^- is significantly smaller than the corresponding measure for the intra-monomer bonds. Hence the IM qualifier following the 3/4 bond orders in Figure 5(a): these 3/4 IM bonds are significantly weaker than, for example, one half of the order-of-1.5 bond in O_2^-.

We can use the known $O_2(^3\Sigma_g^-) \rightarrow O(^3P) + O(^3P)$, $O_2^-(^2\Pi_g) \rightarrow O(^3P) + O^-(^2P)$, and $O_4^- \rightarrow O_2(^3\Sigma_g^-) + O_2^-(^2\Pi_g)$ dissociation energies to quantify this trend. The O_2 dissociation energy of 5.15 eV, corresponding to the O=O double bond, and the O_2^- dissociation energy of 4.10 eV, corresponding to an order-of-3/2 bond, translate into the average intra-monomer bonding strength of ~2.6 eV per bond-order. Given the O_4^- dissociation energy of 0.455 eV [76], corresponding to two IM bonds of 0.75 order each, the IM bonding strength in O_4^- is ~0.30 eV per bond-order, an order of magnitude smaller than for the intra-monomer bonding.

It is this order-of-magnitude difference between the intra- and inter-monomer bonding strengths that allows us to view the IM bonding in O_4^- as a perturbation of the much stronger intra-monomer bonds. In the first-order approximation, one can define the IM bonding without considering its effect on the monomer orbitals. The implied separability of the intra- and inter-monomer interactions is a foundation of the CMMO model, allowing us to draw the simplified IMO diagram in Figure 4.

This approximation has its limits, exemplified—spectacularly—by the O_4^- case. Assuming the separability of the intra- and inter-monomer interactions, the effective intra-monomer bond orders of the two O_2 moieties in O_4^- are 1.75 each, as indicated in Figure 5(a). This is a simple average of 2 and 1.5, the respective bond orders in O_2 and O_2^-. Such averaging is only valid under the implicit assumption that the IM bonding in O_4^- does not affect the intra-monomer bonds. However, if that were strictly the case, the intra-monomer bond lengths in O_4^- would be approximately the average of the bond lengths in O_2 and O_2^- (1.209 Å and 1.339 Å, respectively [63]), which gives 1.274 Å. This differs significantly from the actual intra-monomer bond length in O_4^-, 1.217 Å [61], which is barely (only 0.008Å) larger than in neutral O_2.

To put this result in perspective, assume a linear relationship between the bond length and the bond order. Then, the intra-monomer bond order in O_4^-, implied by the actual 1.217 Å bond length, calculates to be 1.97 (very close to 2 in O_2), instead of 1.75 (predicted based on the assumptions of the first-order CMMO model). That is, the actual bonding strength within the monomers in O_4^- is significantly greater than expected. It is as if the additional electron, which

is supposed to be anti-bonding with respect to the monomer bonds, has almost no effect on the bond order, reducing it by merely 0.03.

The origin of this discrepancy can be traced to the partial breakdown of the assumption that the intra-monomer bonding in O_4^- can be completely decoupled from the IM bonding. The 1.75 bond-order value, calculated as the average of the O_2^- and O_2 bond orders, does not consider the effect of the dimerising interactions on the electronic structure of the O_2 moieties themselves. This is the same type of approximation as that assumed in the time-independent perturbation theory, which calculates the first-order energy correction without accounting for the corresponding changes to the wavefunction. Yet, the IM bonding in O_4^- is due to the overlap of the $\pi_g^*(2p)$ MMOs, which are anti-bonding with respect to the intra-monomer bonds (see the sketches in Figure 4). The IM bonds draw the orbital amplitude into the space between the monomers, partially quenching the intra-monomer anti-bonding character of these orbitals. It can be said that *the inter-monomer bonding character is borrowed from the intra-monomer anti-bonds*, strengthening the intra-monomer bonds as a side effect of the inter-monomer bonding. In the language of the perturbation theory, this is a first-order correction to the wave function and a second-order effect on the bond strength.

Another important point concerning O_4^- further illuminates the limitations of the CMMO approach. The IMO diagram in Figure 4, viewed without the excess (red) electron, might lead one to conclude the existence of a covalently bonded neutral dimer of O_2, the O_4 molecule, with four bonding and zero anti-bonding electrons populating the IMOs, giving it an overall IM bond order of 2. That would correspond to two single O–O bonds between the monomers, consistent with the 1924 prediction by G. N. Lewis, based on the Lewis structure [77]:

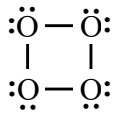

On this basis, one might expect a closed-shell O_4 molecule with four equivalent single O-O bonds, in which the distinction between the intra- and inter-monomer bonds vanishes. The actual bonding in O_4 is more complex. To this day, it continues to draw intense interest and the reader is referred to the literature on the subject [78-81]. In the present context, it suffices to say that a stationary point on the singlet O_4 potential energy surface does exist. The corresponding structure is non-planar (puckered, D_{2d} symmetry), weakly bound, and dissociates into two O_2 molecules [81]. These facts are not in contradiction with the CMMO formalism described above, because the diagram in Figure 4 should not be applied to O_4, for several reasons, including first and foremost the breakdown of the assumed separation of the intra- and intermolecular bonding.

It is revealing that this separation works for O_4^-, but not for O_4. A qualitative explanation of the difference between the two species can be realized by considering the effect of electron detachment from the stable ground-state O_4^- anion, yielding unstable neutral O_4. The O_4^- potential minimum is at a large IM separation (Figure 5(a)), where, based on our analysis, the IM bond integrals are an order of magnitude smaller than the corresponding values for the intra-monomer bonds. According to Figure 4, removal of the excess electron from $\phi_{\mathrm{LVO},2}^*$ (the O_4^- HOMO in the conventional MO theory) increases the IM bond order. That will have an effect of pulling the two O_2 moieties closer together, which, in turn, increases the overlap between

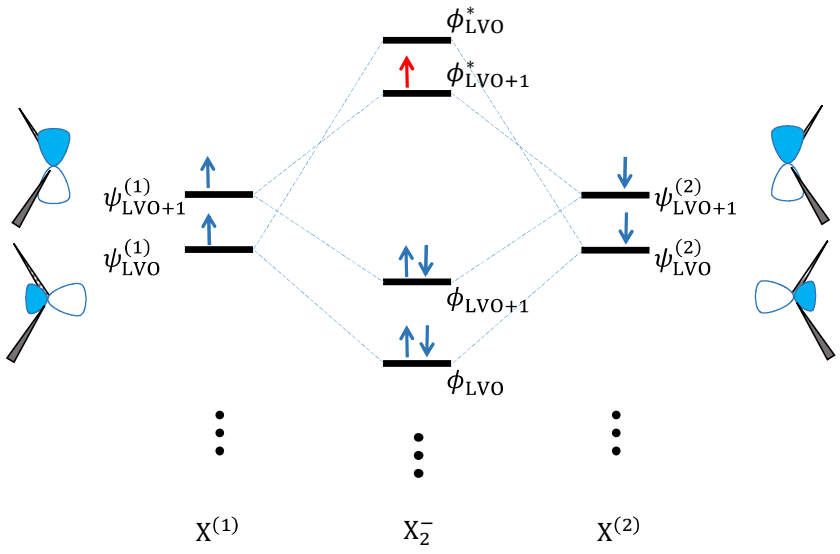

Figure 6. Generic IMO diagram for type-IIb anionic dimerisation. The MMO sketches correspond to triplet ground state carbenes. See the text for details.

the MMOs, thus increasing the magnitude of the IM bond integrals and, therefore, the bond strength, pulling the monomers closer together yet. The thought cycle expressed in the previous run-on sentence continues until the perturbative picture breaks down and the CMMO description becomes inapplicable to the neutral structure. It must, instead, be considered at a significantly higher level of theory [78-81].

Moving on, an IMO diagram for type-IIb dimerisation is shown in Figure 6. In this case, the dimer anion is formed from two triplet-state neutral monomers with nearly, but not exactly degenerate HOMO and HOMO–1, described here as LVO+1 and LVO, respectively. Each of these MMOs contains an unpaired electron. Depending on the relative magnitudes of the IM bond integrals and the LVO/LVO+1 energy splitting, different IMO energy orderings are possible. The diagram in Figure 6 was prepared with the coupling of two triplet-ground-state carbenes in mind, and the orbital sketches shown correspond to that general case. The dimerisation of carbenes is a good model case, because the carbene MMOs contributing to the IMO diagram in Figure 6 are of non-bonding intra-monomer character, allowing us to separate the IM interactions from the intra-monomer bonding and avoid the pitfalls like in the O_4 case.

Relevant examples of type-IIb dimerisation include the already mentioned anionic dimerisation of cyanocarbene (X = HCCN) [72,82-94] to yield the anion of fumaronitrile, fn^- = $(HCCN)_2^-$. The fn^- structure is shown in Figure 7(c) [64]. Another example is a similar reaction involving the dicyano-version of X: the anionic dimerisation of dicyanocarbene (X = NCCCN) [95], yielding the anion of tetracyanoethylene, $(NCCCN)_2^-$ [96]. Both carbenes (HCCN and NCCCN) have triplet ground states and their electron configurations, the bonding caveats, and model limitations are similar to the type-IIa case. Contrary to the case of O_4, however, the IMO diagram in Figure 6 correctly predicts the bonding properties in both the neutral and anion states of fumaronitrile and tetracyanoethylene. For example, for the ground-state singlet fumaronitrile and its anion, Figure 6 predicts the ethylene bonds (treated as IM bonds) to have bond orders of 2 and 1.5, respectively. These predictions are in qualitative agreement with the bond lengths in the structures shown in Figure 7(a) and (c), respectively.

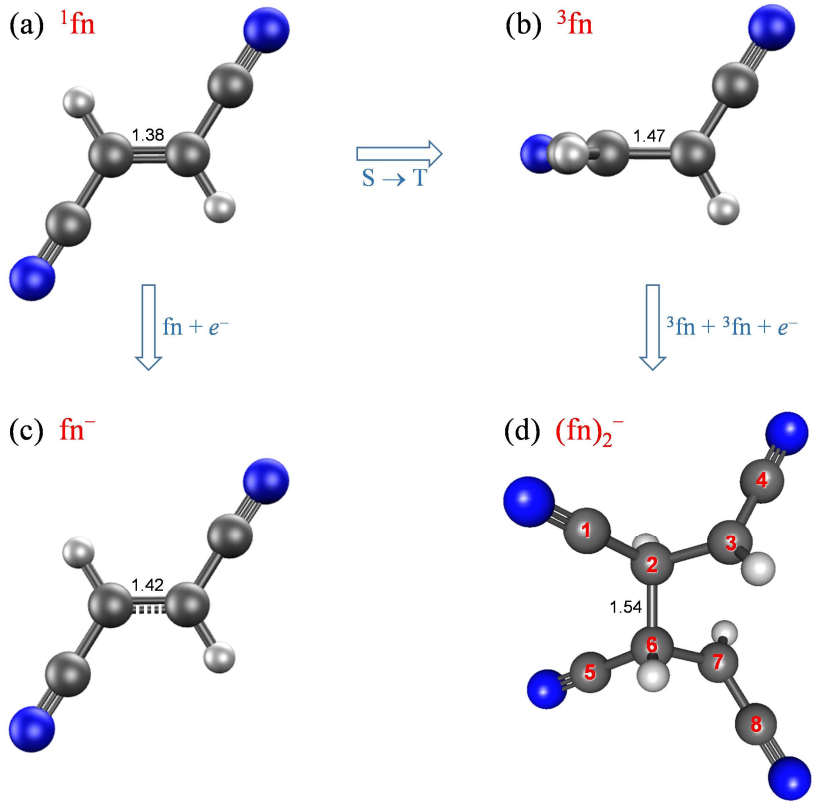

Figure 7. Equilibrium geometries of (a) the singlet-ground-state fumaronitrile (fn); (b) the first excited triplet state of fn; (c) the fn^- anion; and (d) the $(fn)_2^-$ dimer anion. Only the most important geometric parameters are indicated (in Angstroms). The complete structures are reported in Ref. [62].

Even though the strength of the IM double-bond between the HCCN moieties in Figure 7(a) is of the same order of magnitude as the intra-monomer bonds, the separability approximation holds up in this case, because of the non-bonding nature of the triplet carbene's LVO and LVO+1. That is, the bonding overlap of the respective orbitals of the coupled monomers does not significantly affect the bonding within the carbene moieties themselves.

3.2.4. Type III: Charge-sharing dimerisation via singlet-triplet excitation of the monomers

Type-III anionic dimerisation is a curious convolution of the already discussed type-I and type-II cases. It involves monomers that are closed-shell singlets in their ground states (similar to type I), but yield covalent dimer anions whose neutral core configurations are derived from the singlet coupling of the monomers promoted to their respective triplet states (type II). That is, the neutral dimer configurations are of singlet spin multiplicity, but doubly excited with respect to the corresponding van der Waals dimer wave functions.

We will rely on the examples of $(CS_2)_2^-$ and $(OCS)_2^-$ [16,17,19,20,22,25-27] to highlight the qualitative features of type-III dimerisation. The electronic structure of these dimer anions is qualitatively different from $(CO_2)_2^-$, which is remarkable considering that all three monomers in the X = CO_2, OCS, and CS_2 series are isovalent molecules. A generic IMO diagram for the type-III dimerisation, constructed with the X = CS_2 case in mind, is shown in Figure 8. It should be compared to the type-I (X = CO_2) diagram in Figure 2.

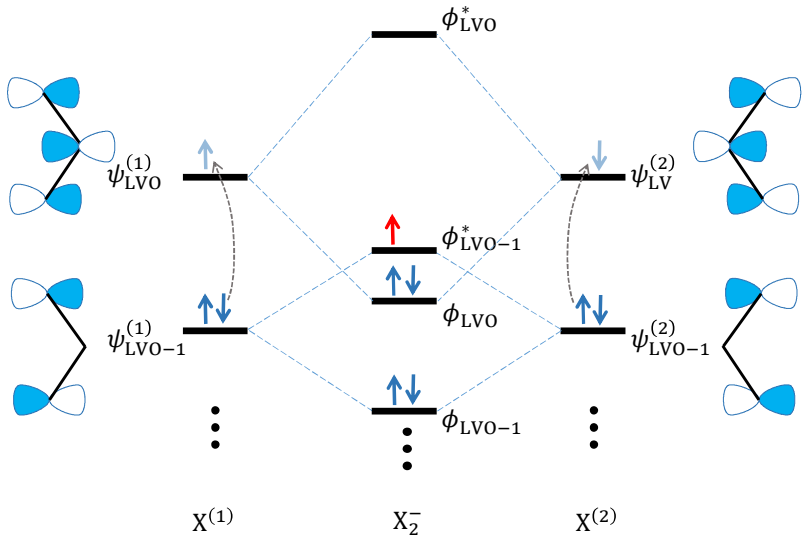

Figure 8. Generic IMO diagram for type-III anionic dimerisation. The MMO sketches correspond to X = CS_2 (or similar molecules) at a bent anion geometry. In the ground singlet states of the neutral monomers, $\psi^{(1)}_{\mathrm{LVO}}$ and $\psi^{(2)}_{\mathrm{LVO}}$ are empty. The pale arrows populating these orbitals in the figure indicate the results of singlet-triplet excitations in the monomers: $\psi^{(1)}_{\mathrm{LVO}-1}\beta \rightarrow \psi^{(1)}_{\mathrm{LVO}}\alpha$ and $\psi^{(2)}_{\mathrm{LVO}-1}\alpha \rightarrow \psi^{(1)}_{\mathrm{LVO}}\beta$.

The distinctions of the diagram in Figure 8 from its counterpart in Figure 2 stem from the smaller energy gap between the active monomer orbitals, LVO−1 and LVO. The reduced gap facilitates the $\psi^{(i)}_{\mathrm{LVO}} \rightarrow \psi^{(i)}_{\mathrm{LVO}}$, i = 1, 2 excitations, indicated by the dashed curved arrows in Figure 8. Although these excitations still cost energy in the isolated monomers, they promote much stronger IM interactions stabilising the dimer species. To take advantage of this stabilisation, $(CS_2)_2^-$ [19,22,25-27] and other type-III dimers adopt planar geometries, contrasting them to the D_{2d} structure of $(CO_2)_2^-$ [9]. In the latter, the IM bonding involves predominantly a long-range overlap between the carbon lobes of $\psi^{(1)}_{\mathrm{LVO}}$ and $\psi^{(2)}_{\mathrm{LVO}}$, while the interactions between the respective oxygen lobes of the same orbitals, as well as between the entire $\psi^{(1)}_{\mathrm{LVO}-}$ and $\psi^{(2)}_{\mathrm{LVO}-1}$ MMOs, are minimal (Figure 2). The C_{2v} and D_{2h} structures of $(CS_2)_2^-$ [25], on the other hand, allow for effective overlaps between both the respective C and S lobes of both MMO types, leading to significantly larger splittings between the resulting bonding/antibonding IMO pairs (Figure 8).

In sum, the $\psi^{(i)}_{\mathrm{LVO}-1}/\psi^{(i)}_{\mathrm{LVO}}$ MMO splitting in $(CS_2)_2^-$ is smaller than that in $(CO_2)_2^-$, while the $\phi_{\mathrm{LVO}}/\phi^*_{\mathrm{LVO}-1}$ and $\phi_{\mathrm{LVO}}/\phi^*_{\mathrm{LVO}}$ IMO gaps are both larger (compare Figure 8 to Figure 2). The combination of the two pushes the $\phi^*_{\mathrm{LVO}-1}$ IMO above ϕ_{LVO}, reversing the order of these orbitals in $(CS_2)_2^-$ versus $(CO_2)_2^-$. Based on the diagram in Figure 8, the nominal type-III electron configuration of $(CS_2)_2^-$ is:

$$\mathrm{X}_2^-\text{: } \ldots(\phi_{\mathrm{LVO}-1})^2(\phi_{\mathrm{LVO}})^2(\phi^*_{\mathrm{LVO}-1})^1 \qquad (7)$$

It should be compared to the type-I configuration of $(CO_2)_2^-$ in Equation (4). Based on Equation (7), the nominal IM bond order in $(CS_2)_2^-$ is 1.5, compared to 1/2 predicted by Equation (4) for $(CO_2)_2^-$. This prediction is indeed correct. For example, the C_{2v} symmetry (cyclic) structures

of $(CS_2)_2^-$ and $(OCS)_2^-$ each feature a single IM bond between the carbon atoms, plus an order-of-1/2 IM bond among *one* pair of S in each case, for a combined IM bond order of 1.5. As also seen in Figure 8, the neutral dimer configuration, indicated by the blue arrows (only) in the middle part of the figure (excluding the excess electron shown in red), correlates to the triplet states of the monomers, i.e., $X_2 \rightarrow {}^3X + {}^3X$, rather than the singlets in Figure 2. This is to say that the core neutral configuration of a type-III dimer is doubly-excited, compared to a pair of closed-shell monomers, and results from singlet-coupling of two ^3X moieties.

To construct the type-III IMO diagram in Figure 8, we started from the type-I case in Figure 2 and revised it based on the comparative properties of $(CS_2)_2^-$ and $(CO_2)_2^-$. The revisions stemmed from the reduced MMO gaps in the type-III case leading, in turn, to increased IM interactions. For other systems, the construction of a type-III diagram may more conveniently (but equivalently) begin from the opposite extreme of type IIb, illustrated in Figure 6. In this alternative approach, the splitting between the active type-III MMOs must be increased, compared to type IIb, reflecting the respective singlet and triplet ground states of the monomers in the two cases. Because of the larger MMO splitting, the IMO ordering will generally be different in type-III dimers, compared to Figure 6, depending on the specific system. Nonetheless, it is easy to see that shifting the $\psi^{(1)}_{\mathrm{LVO}+1}$ and $\psi^{(2)}_{\mathrm{LVO}+1}$ MMO pair and the resulting $\phi_{\mathrm{LVO}+1}$ and $\phi^*_{\mathrm{LVO}+1}$ IMOs in Figure 6 upward in energy, while keeping the $\phi_{\mathrm{LVO}+1}/\phi^*_{\mathrm{LVO}+1}$ gap unchanged, yields an IMO set similar to that in Figure 8. The only (inconsequential) difference concerns the (LVO–1)/LVO/(LVO+1) labels assigned to the monomer orbitals.

The hypothesised dimer anion of fumaronitrile [64] is also an example of a type-III species. Two pieces of experimental evidence suggest covalent bonding between the fn moieties in $(fn)_2^-$ [64]. The first is the large (0.94 eV) photodetachment band shift for $(fn)_2^-$ relative to fn^-. The second is the $(fn)_2^-$ photofragmentation pattern, which is dominated by fn^- fragments. These fragments are consistent with a covalent structure of $(fn)_2^-$ and inconsistent with a solvated $fn^-\cdot fn$ cluster. Because the fn molecule itself, N≡C–C(H)=C(H)–C≡N, is a covalent dimer of cyanocarbene, HCCN (used as a type-IIb example in Section 3.2.3), the $(fn)_2^-$ dimer anion can also be viewed as a tetramer anion of cyanocarbene.

The predicted structure of $(fn)_2^-$ is shown in Figure 7(d) [64]. It has a 1.54 Å bond between two equivalent fn moieties. Its electronic wavefunction is described by the correlation: ${}^3fn + {}^3fn + e^- \rightarrow {}^1(fn)_2^* + e^- \rightarrow {}^2(fn)_2^-$, where the leading superscripts designate the spin-multiplicity and the asterisk sign denotes an excited state. This correlation illuminates the salient details of the dimer-anion structure but (again) is not intended as the $(fn)_2^-$ formation mechanism. In the experiment, $(fn)_2^-$ is likely formed via electron attachment to $(fn)_n$ van der Waals clusters, followed by evaporative cooling and internal conversion to the above $(fn)_2^-$ state [64].

The photodetachment of $(fn)_2^-$ accesses a transient doubly excited neutral ${}^1(fn)_2^*$, which correlates diabatically to the ${}^3fn + {}^3fn$ dissociation limit. All this is similar to the just discussed $(CS_2)_2^-$ case. To avoid repetition and offer a different perspective, we will switch from the previously used MMO basis for the dimer-anion wave functions to the equivalent picture of localised radical centres. Each centre is described by a singly-occupied localised orbital, constructed as a linear combination of the active MMOs. (It is for this reason that the radical-centre description is mathematically equivalent to the IMO picture.) In the localised basis, each of the ${}^3fn$ monomers is a diradical described as N≡C–(H)Ċ–Ċ(H)–C≡N. The ${}^1(fn)_2^*$ state involves four radical centres, nominally located at C2, C3, C6, and C7 in Figure 7(d). Nominally a *quad-*

radical, the $^1(fn)_2^*$ neutral structure, accessed in the lowest-energy photodetachment of $(fn)_2^-$, lends two of the unpaired electrons to the dimerising C2–C6 bond, reducing $^1(fn)_2^*$ to a diradical. The remaining two radical centres (C3 and C7) are separated by a larger spatial gap, because the formation of a symmetric, but strained four-membered carbon ring (C2–C3–C7–C6) is unfavourable compared to the structure shown in Figure 7(d).

Upon anion photodetachment, the unbound radical centres C3 and C7 in Figure 7(d) are involved in through-bond and through-space interactions within the transient neutral species, giving rise to a manifold of closed-shell singlet, triplet, and open-shell singlet states. This is conceptually similar to ring-open oxazole [97] and isoxazole [98], but achieved here in the context of dimerisation rather than ring-opening. The predicted 2.59 Å C3–C7 gap in $(fn)_2^-$ is narrower than the respective 3.06 Å and 3.08 Å inter-radical distances in ring-open oxazole [97] and isoxazole [98]. Therefore, further experiments on $(fn)_2^-$ may provide a striking example of diradical spectroscopy.

We conclude this section with a straightforward recipe for the search for other examples of type-III dimer anions, as well as for predicting the most favourable electronic motif of dimer anions obtained from closed-shell neutral molecules. As discussed above, closed-shell species can yield either type-I or type-III dimers. In the qualitative electronic-structure context, $(fn)_2^-$ is similar to $(OCS)_2^-$ and $(CS_2)_2^-$: they are all based on the singlet-triplet (S-T) excited building blocks [16,25]. This contrasts the famous case of $(CO_2)_2^-$, whose core electron configuration is based on singlet-state monomers [9]. The distinction is attributed to the different magnitudes of the corresponding S-T gaps ($\Delta E_{S\text{-}T}$) in the monomers. For the above cases, $\Delta E_{S\text{-}T}$ is ≤ 2.6 eV in fn [64,99], ~ 3.4 eV and ~ 3.2 eV, respectively, in OCS and CS_2, but a prohibitive ~ 5.3 eV per monomer in CO_2 [16,25]. The $\Delta E_{S\text{-}T}$ values for fn, OCS, and CS_2 prove to be sufficiently small for the combined cost of the S-T excitation of two monomers to be recovered through the covalent bonding and the large electron affinity of the resulting dimer (type-III anionic dimerisation). In $(CO_2)_2^-$, on the other hand, the price of promoting two CO_2 moieties to the triplet state is > 10 eV. This is too high and hence the most stable $(CO_2)_2^-$ structure results from the addition of an electron to the lowest unoccupied IMO of the van der Waals dimer configuration (type-I dimerisation). There are many organic molecules with relatively small S-T gaps and this property can be used to screen the candidates for type-III dimerisation.

4. Hückel-style treatment of cluster anions of closed-shell monomers

We now turn to a quantitative description of one-electron covalent (charge-sharing) and electrostatic (solvation) IM interactions, specifically in clusters allowing for type-I dimerisation or polymerisation. (In type-II and III systems, IM bonding involves more than just the one added electron and must be treated differently.) This section lays out a formalism targeting both types of interactions by pairing the CMMO model with an approximate Hückel-style treatment [100]. The overarching goal is to discover the fundamental limits of the bonding power of one electron added to a system of otherwise non-interacting monomers. The limitations and constraints attributed to real clusters and applications to real-life chemistry are discussed in Section 5.

4.1. *Ion-molecule solvation interactions*

To set the stage, we first tackle the solvation interactions. No necessary role in the treatment of solvation belongs to the original Hückel theory [101-104] or the general MO theory, because

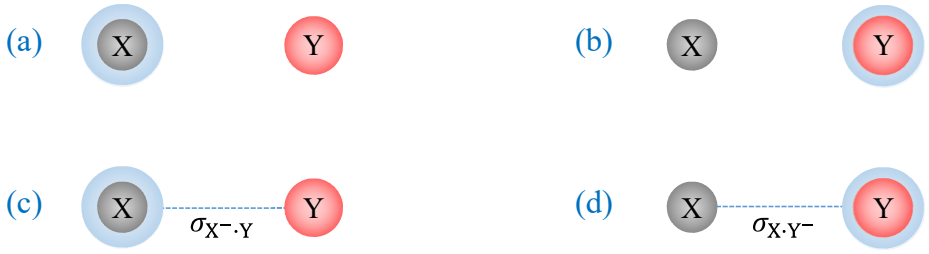

Figure 9. (a)-(b) Schematic representations of the non-interacting $X^- + Y$ and $X + Y^-$ systems, respectively. (c)-(d) Corresponding depictions of the respective solvated $X^-\cdot Y$ and $X\cdot Y^-$ eigenstates, with solvation factors $\sigma_{X^-\cdot Y}$ and $\sigma_{X\cdot Y^-}$, as indicated.

no chemical bonds are formed in noncovalent interactions. The objective in this part is to adapt the familiar MO language and the Hückel-style matrix formalism to the solvation problem, to allow for a subsequent straightforward integration of the covalent and noncovalent forces into one mathematical model.

First, consider a system of two *non-interacting* monomers, X and Y, plus an electron. This description can apply to homogeneous (X = Y) or heterogeneous (X ≠ Y) clusters. Let the LVOs of X and Y be $\psi^{(X)}$ and $\psi^{(Y)}$, respectively. Excluding any *intra*-monomer interactions, the Hamiltonian of this system in the $\{\psi^{(X)}, \psi^{(Y)}\}$ basis is represented by the matrix:

$$\mathbf{H} = \begin{pmatrix} \alpha_X & 0 \\ 0 & \alpha_Y \end{pmatrix} \tag{8}$$

where $\alpha_i = \langle \psi^{(i)} | \hat{H} | \psi^{(i)} \rangle$, i = X, Y, are the Coulomb integrals from the general MO theory, corresponding to the energies of the excess electron bound to X or Y, respectively. If we define the zero of energy to correspond to three non-interacting particles (neutral X and Y, plus an electron at infinity), then in the Koopmans' theorem limit [105] $-\alpha_X$ and $-\alpha_Y$ are the electron affinities (EA) of X and Y. For a stable anion (EA > 0), the Coulomb integral is negative. α_X and α_Y are also the eigenvalues of **H** corresponding to $\psi^{(X)}$ and $\psi^{(Y)}$, respectively. If both are negative, the system has two valence-bound anion states: $X^- + Y$ with $E_1 = \alpha_X$ and $X + Y^-$ with $E_2 = \alpha_Y$, represented in Figure 9(a) and (b), respectively. A superposition of the $(X^- + Y)$ and $(X + Y^-)$ states is not an eigenstate, unless $\alpha_X = \alpha_Y$. If indeed X = Y, then an additional interaction (covalent or other) may lift the degeneracy, with the above superpositions determining the correct zeroth-order wave functions in the degenerate perturbation theory sense.

Next, we allow the monomers to interact via noncovalent (electrostatic) forces only. This stage of the model is applicable to any (predominantly) solvated cluster, such as $I^-\cdot CO_2$. Even for clusters that exist as covalent dimers, such as $(CO_2)_2^-$, $(fn)_2^-$, to understand their stabilities one must compare the covalent species to the alternative solvated structures. Without covalent bonding, the solvated eigenstates are described as $X^-\cdot Y$ and $X\cdot Y^-$. These states are illustrated in Figure 9(c) and (d), respectively. As in the case described by Equation (8), no mixing of the $\psi^{(X)}$ and $\psi^{(Y)}$ MMO is allowed, for that would correspond to a covalent interaction. The only effect of the solvation, as described in the $\{\psi^{(X)}, \psi^{(Y)}\}$ basis, is the additional stabilisation of the $X^-\cdot Y$ and $X\cdot Y^-$ eigenstates relative to the respective $(X^- + Y)$ and $(X + Y^-)$ limits from Equation (8). Let the solvated eigenvalues be $\alpha_X + \sigma_{X^-\cdot Y}$ for the first state, represented in Figure 9(c), and $\alpha_Y + \sigma_{X\cdot Y^-}$ for the second, in Figure 9(d), The quantities $\sigma_{X^-\cdot Y}$ and $\sigma_{X\cdot Y^-}$

describe the solvation effects and we will refer to them as solvation factors. Similar to Coulomb integrals, the solvation factors are negative for attractive interactions. The corresponding Hamiltonian matrix, in the $\{\psi^{(X)}, \psi^{(Y)}\}$ basis, has the form:

$$\mathbf{H} = \begin{pmatrix} \alpha_X + \sigma_{X^-\cdot Y} & 0 \\ 0 & \alpha_Y + \sigma_{X\cdot Y^-} \end{pmatrix} \tag{9}$$

Although, in general, $\sigma_{X^-\cdot Y} \neq \sigma_{X\cdot Y^-}$, Equation (9) describes a trivial interaction regime, because the off-diagonal elements in **H** are zeros. By definition, the $H_{ij} = \langle \psi^{(i)} | \hat{H} | \psi^{(j)} \rangle$, $i \neq j$ elements represent covalent couplings of the monomers, and without such, $H_{ij} = 0$ for $i \neq j$.

A complication in extending this simple picture to larger clusters comes from the dependence of the solvation factors on the cluster geometric structure. Consider a valance-bound cluster anion with n not necessarily identical monomers $X^{(i)}$, $i = 1, \ldots, n$. Assuming no covalent couplings (i.e., no electron sharing), the excess electron can only assume one of the basis $\psi^{(i)}$ LVO states, i.e. be localised on one of the cluster's building blocks. In a general form, the Hamiltonian of such a system in the $\{\psi^{(i)}\}$ basis is represented by:

$$\mathbf{H} = \begin{pmatrix} \alpha_1 + \sigma_1 & 0 & \cdots & 0 \\ 0 & \alpha_2 + \sigma_2 & \cdots & 0 \\ \vdots & \vdots & \ddots & \vdots \\ 0 & 0 & \cdots & \alpha_n + \sigma_n \end{pmatrix} \tag{10}$$

Each of the Coulomb integrals α_i in Equation (10) is an intrinsic property of the corresponding monomer, independent of the cluster structure, or even the presence of other monomers. Each of the solvation factors σ_i, on the other hand, corresponds to (the negative of) the total solvation stabilisation energy associated with placing the excess electron on $X^{(i)}$, at the cluster geometry being considered. Each σ_i is determined by the cumulative interactions of the $[X^{(i)}]^-$ anion with all neutral monomers $X^{(j)}$, $j \neq i$. These interactions depend not only on the monomer identities, but also the geometry of the cluster.

From this point on, we revert to the homogeneous case, i.e., the clusters composed of identical building blocks, with a generic molecular formula X_n^-. Furthermore, we will consider only valence anions, i.e., the cases illustrated in Figure 1(a) and (b), but not (c). Figure 1(b) reflects covalent charge sharing, which will be treated in Section 4.2. Equation (10) assumes no charge sharing and corresponds to Figure 1(a). In this case, n monomer moieties with uncoupled LVOs yields n cluster eigenstates: $\psi^{(i)}$, $i = 1, \ldots, n$. Each corresponds to a different specific monomer binding the electron. Depending on the cluster geometry, these eigenstates may have different energies, but in the homogeneous case they are all described by the same structural formula: $X^-\cdot X_{n-1}$. The Coulomb integrals α_i in Equation (10) are all identical for identical monomers, and hence we can set all $\alpha_i = \alpha$. The solvation factors, however, generally vary from one monomer to another, depending on the cluster geometry. We illustrate this dependence on two simple model cases, both pertaining to a generic noncovalent valence cluster anion consisting of three monomers.

Without charge sharing, the only possible structural formula of such a cluster is $X^-\cdot X_2$. However, there are many distinct geometric possibilities, two of which are illustrated in Figure 10, left. In case (a), the centres of the three monomers form an equilateral triangle and all three solvation factors are equal. If we assume the total solvation energy to be the sum of pairwise

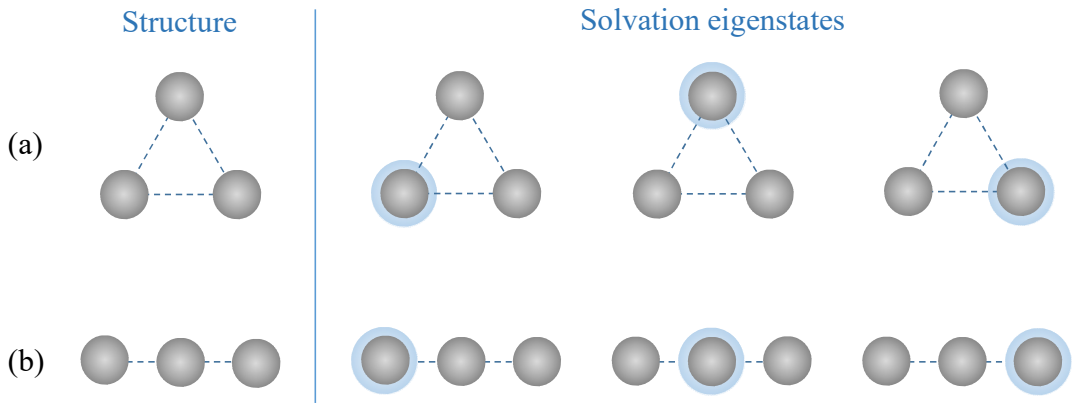

Figure 10. Solvation eigenstates for two different noncovalent X_3^- structures: (a) an equilateral triangle and (b) a linear chain. Dashed lines indicate pairwise interactions.

$X^-{\cdot}X$ ion-neutral interactions, neglecting the neutral-neutral and the many-body terms, then $\sigma_i = 2s$ for $i = 1, 2, 3$, where $s < 0$ in the $X^-{\cdot}X$ pairwise interaction energy. The Hamiltonian matrix, a specific case of Equation (10), then has the form:

$$\mathbf{H} = \begin{pmatrix} \alpha + 2s & 0 & 0 \\ 0 & \alpha + 2s & 0 \\ 0 & 0 & \alpha + 2s \end{pmatrix} \tag{11}$$

The result is three degenerate $X^-{\cdot}X_2$ eigenstates with energy $E_{1-3} = \alpha + 2s$. The electron localisation in each of these states is illustrated on the right side of Figure 10(a).

Case (b) in Figure 10 corresponds to a chain $(X{\cdot}X{\cdot}X)^-$ structure, with two distinct types of monomer locations: the ends of the chain, where the monomer ($i = 1$ or 3) interacts directly only with one other X moiety ($\sigma_1 = \sigma_3 = s$), and the centre, where the monomer ($i = 2$) interacts with two moieties ($\sigma_2 = 2s$). The **H** matrix then has the form:

$$\mathbf{H} = \begin{pmatrix} \alpha + s & 0 & 0 \\ 0 & \alpha + 2s & 0 \\ 0 & 0 & \alpha + s \end{pmatrix} \tag{12}$$

It yields a non-degenerate $X{\cdot}X^-{\cdot}X$ ground state with the energy eigenvalue $E_2 = \alpha + 2s$, and two degenerate excited states, $X^-{\cdot}X{\cdot}X$ and $X{\cdot}X{\cdot}X^-$, with $E_{1,3} = \alpha + s$. The corresponding eigenfunctions are illustrated on the right side of Figure 10(b).

4.2. Charge-sharing polymerisation

We now consider the covalent IM interactions in cluster anions, limiting the discussion to Type-I species defined in Sections 3.2.1 and 3.2.2. Since only valence anions fall under this classification, the following analysis is not applicable to dipole-bound states, solvated-electron clusters, or other species in which valence monomer orbitals are not involved in binding the excess electron. Specifically in the type-I case, the electron binds to a bonding superposition of the monomer LVOs, which is empty in the neutral state (Figure 2), creating an order-of-1/2 covalent bond character shared among all the monomers involved.

4.2.1. Covalent dimer anions of closed-shell molecules

First, consider the formation of a covalent bond between two monomers that are closed-shell species in their respective neutral states. This scenario corresponds to many known type-I dimers, including $(CO_2)_2^-$.

The dimerising bond in X_2^- is due to the excess electron entering the IMO system, which is defined by the Hückel-style Hamiltonian matrix [40]:

$$\mathbf{H} = \begin{pmatrix} \alpha & \beta_{1/2} \\ \beta_{1/2} & \alpha \end{pmatrix} \tag{13}$$

This representation is defined in the $\{\psi^{(i)}\}$ basis, where $\psi^{(i)} = \psi^{(i)}_{\mathrm{LVO}}$ are the $X^{(i)}$ LVOs (i = 1, 2) responsible for the IM bond formation. For example, for $(CO_2)_2^-$, $\psi^{(1)}$ is represented by the top left MMO sketch in Figure 2 ($\psi^{(1)}_{\mathrm{LVO}}$), while $\psi^{(2)}$ corresponds to the top right sketch ($\psi^{(2)}_{\mathrm{LVO}}$) in the same figure. For the biacetyl dimer anion, $\psi^{(1)}$ is the MMO shown in Figure 3(a), while $\psi^{(2)}$ is the same orbital on the second monomer. The Coulomb integral α in Equation (13) is defined the same way as in Section 4.1: $\alpha = \langle\psi^{(i)}|\hat{H}|\psi^{(i)}\rangle$. It corresponds to the MMO energy and has the same value for each of the identical monomers. The off-diagonal elements in Equation (13) describe the bond formation by means of the bond integral $\beta_{1/2} = \langle\psi^{(i)}|\hat{H}|\psi^{(j)}\rangle$. The subscript 1/2 indicates that this specific integral describes an order-of-1/2 IM bond.

The eigenvalues of **H** in Equation (13), $E_{1,2} = \alpha \pm \beta_{1/2}$, are the dimer IMO energies. Only one electron populates the IMO system described by Equation (13) in a type-I dimer anion. Since the bonding in X_2^- is due to the stabilisation of this electron relative to the isolated monomer orbital, the bond dissociation energy can be calculated as the difference between α and the smallest IMO eigenvalue, $E_1 = \alpha + \beta_{1/2}$. The bond energy is, therefore, $-\beta_{1/2}$, where the minus sign accounts for the negative value of the bond integral. This energy does not account for the vibrational relaxation of (molecular) monomers upon the IM bond formation. Therefore, it is described as *vertical* stabilisation energy, VSE = $-\beta_{1/2}$.

The eigenvectors of **H** contain the coefficients representing the IMOs in the MMO basis. The normalized eigenvector for the lowest eigenvalue of **H** in Equation (13) is $\left(1/\sqrt{2}, 1/\sqrt{2}\right)$. It reflects equal contributions of the MMOs, $\psi^{(1)} = \psi^{(1)}_{\mathrm{LVO}}$ and $\psi^{(2)} = \psi^{(2)}_{\mathrm{LVO}}$, to the bonding IMO, ϕ_{LVO}, and an even, –0.50/–0.50, charge sharing between the monomers. This is consistent with the properties of $(CO_2)_2^-$ [9] and other covalent dimer anions [40].

4.2.2. Covalent trimer anions of closed-shell molecules

We will now analyse two sample X_3^- structures shown on the left side of Figure 10. Unlike the case of pure solvation (Section 4.1), the covalent eigenstates will have a delocalised structure, and so the eigenstate sketches on the right side of Figure 10 do not apply. Furthermore, we will change the order and first consider the chain (or stacked) anion structure $[X\text{-}X\text{-}X]^-$ shown in Figure 10(b), and only then turn our attention to the triangular arrangement in Figure 10(a).

The stacked trimer structure in Figure 10(b) possesses a distinct central moiety, bound to two equivalent end monomers. Such structures have been proposed for π-stacked trimer anions of organic molecules, e.g., tetrachloroquinone [106] and biacetyl [68]. Other systems may seem as plausible candidates for such covalent trimers, but form $X_2^-{\cdot}X$ structures instead. In the

triangular X_3^- structure shown in Figure 10(a), all three X moieties are equivalent. Such a trimer can be envisaged for CO_2, but it is less stable than the $(CO_2)_2^-{\cdot}CO_2$. The recently reported $(CO)_3^-$ trimer [107] is an actual example of a triangular structure, with the caveat that under our classification it is a type-III (not type-I) species (see Section 3).

A triple-decker [X-X-X]$^-$ structure has two IM bonds. The order-of-1/2 bonding character due to a single electron populating the bonding IMO in this structure is shared among the two equivalent X-X bonds, yielding a nominal bond order of 1/4 for each. (Unless stated otherwise, we will continue using the Lewis-style bond orders, rather than those calculated from the Hückel-style eigenvectors [100].) Similar to the dimer anion (Section 4.2.1), the IM bonding in the stacked trimer results from a bonding overlap of the MMOs: $\phi = \sum c_i \psi^{(i)}$, where ϕ is the trimer IMO and $\psi^{(i)}$, $i = 1 - 3$, are the LVOs of the neutral monomers. As an example, the trimer IMO for biacetyl, first reported in Ref. [68], is shown in Figure 3(c). The Hückel-style Hamiltonian matrix for [X-X-X]$^-$ in the $\{\psi_{\mathrm{LVO}}^{(i)}\}$ basis has the form [40]:

$$\mathbf{H} = \begin{pmatrix} \alpha & \beta_{1/4} & 0 \\ \beta_{1/4} & \alpha & \beta_{1/4} \\ 0 & \beta_{1/4} & \alpha \end{pmatrix} \tag{14}$$

The Coulomb integrals α in Equation (14) are the same as in other cases, depending only on the nature of X, but the bond integrals are distinct in value from the ones used in the dimer case. As indicated by the subscript, $\beta_{1/4}$ in Equation (14) corresponds to a 1/4-bond, while $\beta_{1/2}$ in Equation (13) to a 1/2-bond.

The bond orders (BO) are used here as mere labels; their use is not meant to imply that the bond integrals β_{BO} depend explicitly on BO. They do not. The bond order is a secondary construct, determined by the populations of the IMOs obtained by diagonalising the Hamiltonian. As in the conventional Hückel theory, the same **H** matrix can describe systems with different bond orders, depending on the number of electrons populating the MO or IMO system. For example, recall that the π systems of ethylene, $H_2C{=}CH_2$, and its cation are described by the same Hückel matrix, but the corresponding bond orders are different, due to the different numbers of electrons in each case.

That said, the bond integrals, generally written as β_{ij}, are defined as $\beta_{ij} = \langle \psi^{(i)} | \hat{H} | \psi^{(j)} \rangle$, $i \neq j$, where $\{\psi^{(i)}\}$ is the MMO basis. By this definition, they depend on the MMO overlap and, therefore, the IM separation, which in turn depends on the bond order. Therefore, β_{BO} do depend on BO, just not explicitly. In the language of multivariable calculus, one might say that $\partial\beta_{\mathrm{BO}}/\partial(\mathrm{BO}) = 0$, but $d\beta_{\mathrm{BO}}/d(\mathrm{BO}) \neq 0$. Since the bond length generally increases with decreasing BO, we should expect β_{BO} to decrease in magnitude, due to the decreasing MMO overlap. Specifically, $|\beta_{1/4}| < |\beta_{1/2}|$, but the difference is subtle, not scaling linearly with BO. For example, it would be incorrect to expect $\beta_{1/4}$ to be approximately one-half of $\beta_{1/2}$.

The eigenvalues of **H** in Equation (14) are (in increasing order): $E_1 = \alpha + \sqrt{2}\beta_{1/4}$, $E_2 = \alpha$, and $E_3 = \alpha - \sqrt{2}\beta_{1/4}$. Only the lowest-energy IMO is populated by an electron in [X-X-X]$^-$, resulting in two 1/4-IM bonds. The interaction energy, reflecting the combined energy of both bonds, is VSE = $\alpha - E_1 = -\sqrt{2}\beta_{1/4}$. If $\beta_{1/4}$ and $\beta_{1/2}$ were equal, this would represent a 40% increase in the covalent interaction energy in the trimer, compared to the dimer

anion. Since in fact $|\beta_{1/4}| < |\beta_{1/2}|$, the additional stabilisation of [X-X-X]$^-$, compared to [X-X]$^-$, is even smaller than 40%.

The normalized eigenvector corresponding to the bonding IMO given by Equation (14) is $(1/2,\ 1/\sqrt{2},\ 1/2)$. Neglecting the coupling with other electrons in the trimer, the monomer charges in [X-X-X]$^-$ are –0.25/–0.50/–0.25. In comparison, the overall charges of the monomers in the triple-decker $(ba)_3^-$ structure from Figure 3(c), as determined by the iterative Hirshfeld procedure [108-110], are –0.17/–0.65/–0.17 [40]. Their deviation from the above CMMO prediction yield important insight into the mixing of the covalent and solvated cluster structures, as discussed in Section 5.4.

To complete the discussion of the trimer models in Figure 10, in the cyclic structure shown on the left in (a) all three moieties are equivalent and each of the three IM bonds has an order of 1/6. This reflects the sharing of the order-of-1/2 bonding character due to a single IMO electron between three equivalent IM bonds. The Hamiltonian matrix has the form [40]:

$$\mathbf{H} = \begin{pmatrix} \alpha & \beta_{1/6} & \beta_{1/6} \\ \beta_{1/6} & \alpha & \beta_{1/6} \\ \beta_{1/6} & \beta_{1/6} & \alpha \end{pmatrix} \tag{15}$$

Based on the above arguments, $|\beta_{1/6}| < |\beta_{1/4}| < |\beta_{1/2}|$. The eigenvalues for the matrix in Equation (15) are $E_1 = \alpha + 2\beta_{1/6}$ and $E_{2,3} = \alpha - \beta_{1/6}$, with E_1 being the lowest. Population of the ϕ_1 IMO by one electron results in a VSE = $\alpha - E_1 = -2\beta_{1/6}$.

4.2.3. Anionic tetramers (and beyond) of closed-shell molecules

We now extend the CMMO analysis to the chain tetramer anion structure. Similar treatments of other possible geometries are straightforward and some non-chain structures can be obtained as specific cases on the general multi-dimensional analysis in Sections 4.2.4 and 4.2.5.

The [X$^{(1)}$-X$^{(2)}$-X$^{(3)}$-X$^{(4)}$]$^-$ structure has three IM bonds. Assuming that all four X building blocks are the same, by symmetry, the X1-X2 and X3-X4 bonds are equivalent, but X2-X3 is distinct. Nonetheless, we will assume, as in the conventional Hückel theory, that all three bond integrals describing this structure are the same. Since one bonding electron shared among the three IM bonds results in a 1/6 bond order for each, on average, we will give these bond integrals the $\beta_{1/6}$ designation. The Hückel-style Hamiltonian matrix, expressed in the usual $\{\psi_{\mathrm{LVO}}^{(i)}\}$, $i = 1 \ldots 3$, basis set, has the form [40]:

$$\mathbf{H} = \begin{pmatrix} \alpha & \beta_{1/6} & 0 & 0 \\ \beta_{1/6} & \alpha & \beta_{1/6} & 0 \\ 0 & \beta_{1/6} & \alpha & \beta_{1/6} \\ 0 & 0 & \beta_{1/6} & \alpha \end{pmatrix} \tag{16}$$

The four eigenvalues are $E_{1-4} = \alpha \pm \beta_{1/6}\,(\sqrt{5} \pm 1)/2$, with $E_1 = \alpha + \beta_{1/6}\,(\sqrt{5} + 1)/2$ being the lowest. The normalised eigenvector corresponding to the ϕ_1 IMO evaluates to (0.372, 0.602, 0.602, 0.372), which translates into the –0.14, –0.36, –0.36, –0.14 monomer charges.

Population of ϕ_1 by one electron results in the three weak IM bonds, with a combined VSE = $\alpha - E_1 = -\beta_{1/6}\,(\sqrt{5} + 1)/2 \approx -1.62\beta_{1/6}$. Even with assuming $\beta_{1/6} \approx \beta_{1/4}$, this VSE

represents only a 15% increase in the overall stabilisation energy for the tetra-decker anion, compared to its triple-decker counterpart.

Here and above, we noted that increasing the size (n) of covalently bound chain anions leads to only moderate stepwise increases in their stability relative to the complete dissociation limit, $X^- + (n-1)X$. Even assuming unchanging values of the bond integrals β_{BO} for the progressively decreasing bond orders, the complete dissociation energies of the chain dimer, trimer, and tetramer anions scale as 1:1.41:1.62. Similar calculations on larger X_n^- chain anions show that the 15% increase for the tetramer compared to the trimer is followed by only a 7% increase for the pentamer compared to the tetramer and a mere 4% increase from $n = 5$ to 6.

What's more, these diminishing increases in the dissociation energy assume unchanging bond integral values, and that is a rather crude approximation. We should expect $|\beta_{1/6}|$ to be smaller than $|\beta_{1/4}|$, and the subsequent integral to be smaller than $|\beta_{1/6}|$, etc., so the stabilisation benefits of additional bonds (all carried by the same lone electron) become vanishing indeed. From the energetics standpoint, in larger clusters (beyond the dimer or the trimer) it becomes more favourable to add neutral *solvent* monomers instead of spreading the excess electron ever so thin among the increasing number of progressively weaker covalent bonds.

Despite the crudeness of the unvarying-β_{BO} approximation, it is useful for determining the limits of the bonding power of a single electron in progressively larger type-I systems approaching the bulk limit. This insight is sought in Sections 4.2.4 and 4.2.5.

4.2.4. Anionic arrays of different shapes and sizes

Although the addition of an electron to a network of closed-shell monomers triggers a straightforward mechanism for anionic polymerisation, the size of such "polymers" is limited. As we aim to understand why, the answer comes down to the limited bonding power of one electron and the geometric constraints (Section 5). To arrive at that conclusion, we explore the fundamental limits of one-electron bonding in hypothetical type-I structures of different dimensions, generalising the findings to arbitrary clusters in Section 4.2.5.

First, consider a system of n monomers evenly spaced along a one-dimensional chain, as shown in Figure 11. The shape of the chain is not important: the particles can be arranged on a straight line (a) or be spaced along a curved string (b). As in the previous examples, the bonding among the monomers is due to one excess electron entering the lowest-energy IMO, ϕ_1, defined in the usual $\{\psi_{LVO}^{(i)}\}$, $i = 1 \ldots n$, basis of identical monomer LVOs as $\phi_1 = \sum c_i \psi_{LVO}^{(i)}$. This model was recently explored for small stacked anions of organic molecules, such as

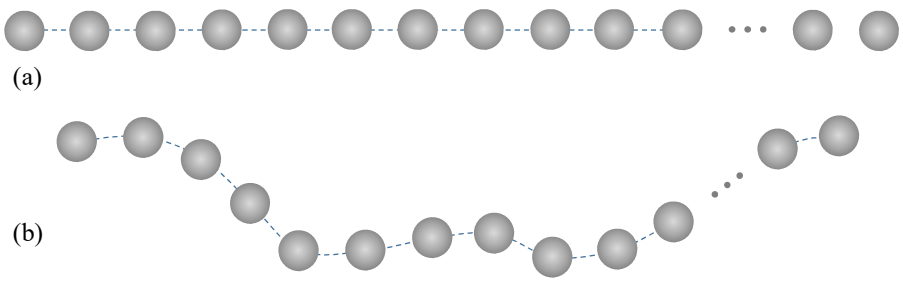

Figure 11. (a) Straight and (b) curved X_n^- monomer arrays. Blue dashes represent nearest-neighbour covalent interactions with bond integral β.

glyoxal or biacetyl [40]. The discussion here is a natural extension to larger clusters, aiming to explain why the growth of type-I chains is fundamentally limited.

Only the nearest-neighbour interactions described by bond integral β are considered and no interactions between non-sequential monomers (e.g., due to chain folding) are allowed. In the $\{\psi_{\mathrm{LVO}}^{(i)}\}$ basis, the system is described by the Hückel-style Hamiltonian matrix, which is a straightforward extension of Equations (13), (14), and (16). All main-diagonal elements are represented by identical Coulomb integrals α, while the adjacent elements are all equal to β:

$$\mathbf{H} = \begin{pmatrix} \alpha & \beta & 0 & \cdots & 0 & 0 \\ \beta & \alpha & \beta & \cdots & 0 & 0 \\ 0 & \beta & \alpha & \ddots & 0 & 0 \\ \vdots & \vdots & \ddots & \ddots & \ddots & \vdots \\ 0 & 0 & 0 & \ddots & \alpha & \beta \\ 0 & 0 & 0 & \cdots & \beta & \alpha \end{pmatrix} \tag{17}$$

As before, the overall stabilisation due to charge sharing is equal to the energy difference between the $X^- + (n-1)X$ limit (i.e., the Coulomb integral α) and the lowest **H** eigenvalue: VSE = $\alpha - E_1$. The general eigenvalue problem for Equation (17) can be solved numerically for any integer n, and we have done so for up to n = 8000, using a custom script coded in MATLAB [111]. Some of the results are shown in Figures 12 and 13. The grey colour in Figure 12 corresponds to the one-dimensional (1-D) covalent stabilisation curve, VSE(n), plotted for clarity against two different horizontal scales: $\log_2 n$ in (a) and linear n in (b). Confirming and expanding the already noted trend, as n increases, VSE(n) levels off at VSE $\rightarrow 2|\beta|$, reaching within 5% of the asymptotic value with as few as n = 9 monomers.

In the limit of $n \rightarrow \infty$, the ground-state wave function becomes indistinguishable from the ground state of the particle in a one-dimensional box. To illustrate this, in Figure 13 we plot the $c_i, i = 1 \ldots n$, coefficients of the eigenvector corresponding to the lowest energy eigenvalue for the case of n = 100 monomers (black open symbols). The corresponding wave function, i.e. the ground-state IMO, is represented as $\phi = \sum c_i \psi_{\mathrm{LVO}}^{(i)}$, where $\psi_{\mathrm{LVO}}^{(i)}$ are the identical LVOs of the evenly spaced monomers. For comparison, the ground-state wave function for the "box"

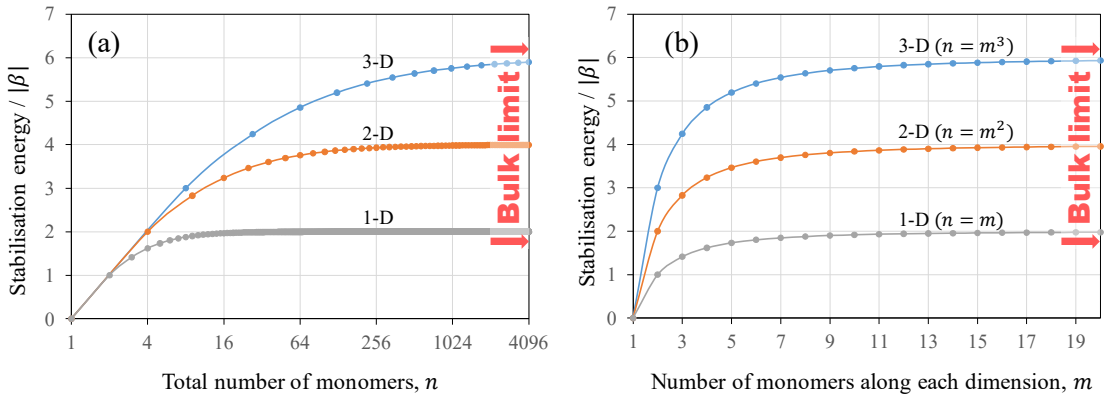

Figure 12. Vertical stabilisation energies (VSE) calculated for the evenly spaced 1-D (chain), 2-D (square), and 3-D (cubic) type-I anionic arrays consisting of $n = m^D$ monomers, where D is the number of spatial dimensions. (a) Total VSE plotted against n on the $\log_2 n$ scale. (b) The same VSE values plotted on the linear m scale.

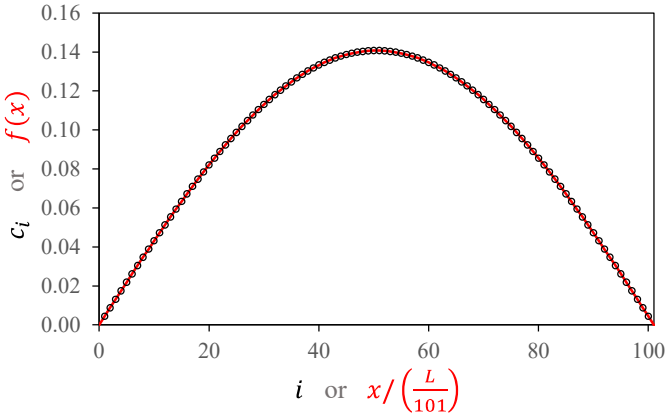

Figure 13. Black symbols: Eigenvector coefficients (c_i, $i = 1 \ldots n$) corresponding to the lowest energy eigenvalue of **H** in Equation (17) with n = 100. This eigenvector describes the lowest-energy bonding IMO of a type-I X_{100}^- chain anion. Red solid curve: the ground-state wave function $f(x) = \sqrt{2/L}\sin(\pi x/L)$ of the particle in the one-dimensional "box" defined by the length of the chain, L.

with the boundaries defined by the length (L) of the X_{100}^- chain, $f(x) = \sqrt{2/L}\sin(\pi x/L)$, is shown using a red solid line in the same figure. The discrete c_i coefficients and continuous function $f(x)$ follow the same trend because the coefficients represent a discretisation of $f(x)$ in the $\{\psi_{\mathrm{LVO}}^{(i)}\}$, $i = 1 \ldots n$, basis. Although this trend is expected for the present model, the ab initio structures of the glyoxal and biacetyl cluster anions revealed notable deviations from the particle-in the-box behavior [40]. In the manner disucssed in Section 5.4, these deviations signal solvation-mediated couplings among various resonance structures.

We now extend the 1-D model to two dimensions (2-D), using the same nearest-neighbour bonding assumption. Envisage adding an electron to an $m \times m$ surface lattice of $n = m^2$ non-interacting neutral monomers, arranged as shown in Figure 14(a). In the $\{\psi_{\mathrm{LVO}}^{(i)}\}$, $i = 1 \ldots n$ basis, the system of $n = m \times m$ monomers is described by an $n \times n$ Hamiltonian matrix containing m^4 elements. Even very large matrices present little difficulty for computers, but they do tend to put a damper on conceptual understanding. For tutorial reasons, we will first illustrate the approach using a small 3×3 array shown in Figure 14(b). All monomers are indexed (sequentially, row-by-row) with $i = 1 \ldots 9$. The corresponding 9×9 matrix is:

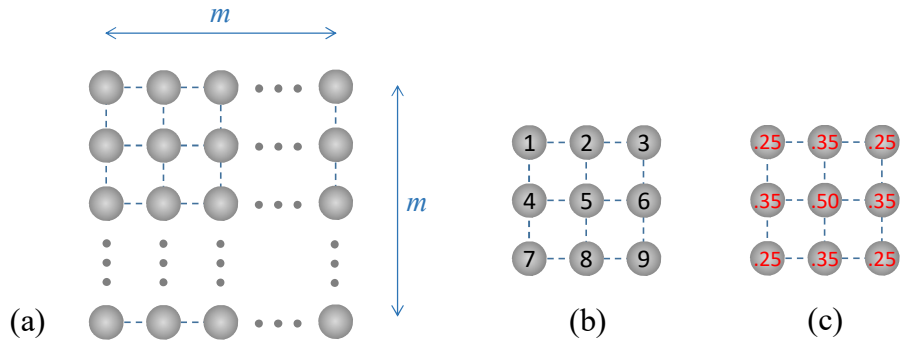

Figure 14. (a) An $m \times m$ surface lattice of $n = m^2$ monomers. (b) A 3×3 monomer array, with the monomers indexed sequentially, row-by-row with $i = 1 \ldots 9$, as indicated. (c) Eigenstate coefficients for the individual $\psi_{\mathrm{LVO}}^{(i)}$ basis functions for the array from (b), indicated in red. The blue dashes in (a)-(c) represent nearest-neighbour covalent interactions with bond integral β.

$$\mathbf{H} = \begin{pmatrix} \alpha & \beta & 0 & \beta & 0 & 0 & 0 & 0 & 0 \\ \beta & \alpha & \beta & 0 & \beta & 0 & 0 & 0 & 0 \\ 0 & \beta & \alpha & 0 & 0 & \beta & 0 & 0 & 0 \\ \beta & 0 & 0 & \alpha & \beta & 0 & 0 & 0 & 0 \\ 0 & \beta & 0 & \beta & \alpha & \beta & 0 & \beta & 0 \\ 0 & 0 & \beta & 0 & \beta & \alpha & 0 & 0 & \beta \\ 0 & 0 & 0 & \beta & 0 & 0 & \alpha & \beta & 0 \\ 0 & 0 & 0 & 0 & \beta & 0 & \beta & \alpha & \beta \\ 0 & 0 & 0 & 0 & 0 & \beta & 0 & \beta & \alpha \end{pmatrix} \tag{18}$$

The lowest eigenvalue, $E_1 = \alpha + 2.828\beta$, corresponds to an interaction energy of VSE = $\alpha - E_1 = -2.828\beta$. The corresponding eigenstate coefficients for the individual $\psi_{\mathrm{LVO}}^{(i)}$ basis functions are indicated in red on top of the corresponding monomers in Figure 14(c). As in the 1-D case, the coefficients reflect a 3×3 discretisation of the ground-state wave function of a particle in a 2-D square box. Increasing m leads to gradual decrease in the pixilation, and in the $m \to \infty$ limit the discretised $m \times m$ eigenstate becomes indistinguishable from the continuous particle-in-the-box wave function.

Extending the protocol to an $m \times m$ array of arbitrary size, the eigenvalue problem was solved numerically for m up to 90, which corresponds to n = 8100 monomers and 6.561×10^7 matrix elements. The resulting 2-D stabilisation curve is plotted in orange in Figure 12(a) with respect to n and in Figure 12(b) with respect to m. As the array size increases, the curve tends towards the VSE $\to 4|\beta|$ asymptote, reaching within 5% for n = 81 (a 9×9 array).

In three dimensions (3-D), consider adding an electron to a cubic $m \times m \times m$ lattice of $n = m^3$ closed-shell monomers. The system is described by an $n \times n$ matrix of m^6 elements. Explicitly writing it out even for a 3×3×3 array (analogous to the above 3×3 case) is impractical, for that would be a 27×27 matrix with 729 elements. For a tutorial illustration, we explicitly consider the 2×2×2 cube array shown in Figure 15. The corresponding matrix is:

$$\mathbf{H} = \begin{pmatrix} \alpha & \beta & \beta & 0 & \beta & 0 & 0 & 0 \\ \beta & \alpha & 0 & \beta & 0 & \beta & 0 & 0 \\ \beta & 0 & \alpha & \beta & 0 & 0 & \beta & 0 \\ 0 & \beta & \beta & \alpha & 0 & 0 & 0 & \beta \\ \beta & 0 & 0 & 0 & \alpha & \beta & \beta & 0 \\ 0 & \beta & 0 & 0 & \beta & \alpha & 0 & \beta \\ 0 & 0 & \beta & 0 & \beta & 0 & \alpha & \beta \\ 0 & 0 & 0 & \beta & 0 & \beta & \beta & \alpha \end{pmatrix} \tag{19}$$

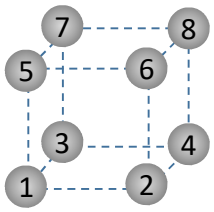

Figure 15. A cubic 2×2×2 array, with the monomers indexed sequentially row-by-row and layer-by-layer. Blue dashes represent nearest-neighbour interactions with bond integral β.

Its lowest eigenvalue $E_1 = \alpha + 3\beta$ corresponds to VSE = -3β, with the eigenstate coefficients all equal to 0.35.

Extending the protocol to an $m \times m \times m$ array of arbitrary size, the eigenvalue problem was solved numerically for m up to 20, corresponding to n = 8000 monomers and 6.4×10^7 matrix elements. The 3-D stabilisation curves, VSE(n) and VSE(m), are plotted in Figures 12(a) and (b), respectively, in blue. As the array size increases, VSE approaches the $6|\beta|$ limit, reaching within 5% of the asymptotic value for n = 729 monomers (a 9×9×9 array).

4.2.5. Generalisation of the charge-sharing trends

At the first glance, the asymptotic bulk limits in Figure 12 appear to scale with the number of spatial dimensions D:

$$\lim_{n\to\infty} \mathrm{VSE}(n; D) = \lim_{m\to\infty} \mathrm{VSE}(m; D) = D \times 2|\beta| \tag{20}$$

(The semicolon indicates that D is a parameter rather than a variable.) Upon closer examination, the above proportionality applies not only to the asymptotes, but to all VSE values. In Figure 12(b), the entire 2-D curve is equal to its 1-D counterpart multiplied by 2: $\mathrm{VSE}(m; 2) = 2 \times \mathrm{VSE}(m; 1)$. Similar for 3-D vs. 1-D: $\mathrm{VSE}(m; 3) = 3 \times \mathrm{VSE}(m; 1)$. Overall, the D-dimensional interaction model for electron binding to an evenly spaced chain/square/cubic X_n lattice, where $n = m^D$, is generalised as follows:

$$\mathrm{VSE}(m; D) = D \times \mathrm{VSE}(m; 1) \tag{21}$$

The result in Equation (21) could be expected, because the spatial coordinates of a D-dimensional lattice of monomers are separable. The right side of Equation (20), on the other hand, requires a closer look, for it relies on the assumptions that we have made about the lattice geometry and the interaction (bond) integrals.

The D×2 multiplier in front of $|\beta|$ on the right side of Equation (20) should be interpreted not as a dimensional property, but as the number of nearest neighbours, $N = 2D$, to which each monomer is bonded within the bulk of a D-dimensional lattice. We will refer to the monomers that are surrounded by other monomers on all sides, i.e., do not belong to a boundary or interface, as "internal". Referring to the cases considered so far, each internal member of a D = 1 chain (Figure 11) is bonded to $N = 2 = 2D$ nearest neighbours; each internal member of the D = 2 square lattice (Figure 14(a)) is bonded to $N = 4 = 2D$ neighbours; and each internal member of the D = 3 cubic lattice is bonded to $N = 6 = 2D$ neighbours. With that, $D \times 2|\beta|$ in Equation (20) is the absolute sum of all bond integrals connected to an internal monomer, which can be generalised even for non-equivalent bonds, as follows:

$$\lim_{n\to\infty} \mathrm{VSE}(n) = -\sum_{q=1}^{N} \beta_q \tag{22}$$

In this equation, the sum is with respect to all bonds formed by an internal monomer and the negative sign accounts for the opposite signs of VSE and the bond integrals.

The result in Equation (22) states that the bonding power of one electron added to a lattice of otherwise non-interacting monomers is a sum of all bonds a single internal monomer can form. To illustrate this, we revisit the 2-D lattice, with the following modification: in addition

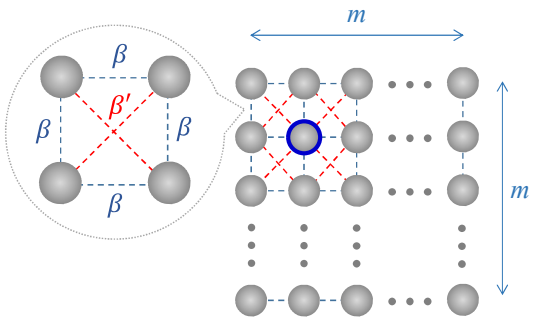

Figure 16. 2-D square lattice array from Figure 14(a), with the diagonal interactions indicated by red dashes included in addition to the nearest-neighbour bonds (blue dashes). All nearest-neighbour interactions are assigned bond integral β, while the diagonal interactions are described by β'. The blue circle around one of the monomers indicates an example of an "internal" monomer.

to the nearest-neighbour bonds (blue dashes in Figure 14(a)), we include the diagonal interactions indicated by the red dashes in Figure 16. As before, all nearest-neighbour interactions are assigned the same bond integral β (blue dashes, also included in Figure 16), while the diagonal interactions (red dashes) are described by β'. Figure 16 also gives an example of an internal monomer, which is highlighted with a blue outline. For this modified interaction model, Figure 17(a) shows three stabilisation curves, calculated with different relative values of β and β'.

The lower curve in Figure 17(a) corresponds to $\beta' = 0$. With null diagonal interactions, it is identical to the 2-D curve in Figure 12(a) and reaches the asymptotic limit of $4|\beta|$. Per Equation (22), it corresponds to the absolute sum of the four nearest-neighbour bond integrals assigned to an internal monomer: $\lim_{n\to\infty} \mathrm{VSE}(n) = -\sum_{q=1}^{N} \beta_q = -(4\beta + 4\beta') = -4\beta = 4|\beta|$ (since $\beta < 0$). The uppermost curve in Figure 17(a) corresponds to each internal monomer connected to all 8 of its nearest and diagonal neighbours by bonds of equal strengths, $\beta' = \beta$. The asymptotic limit of $8|\beta|$ is again equal to the negative of the sum of all bond integrals assigned to an internal monomer: $\lim_{n\to\infty} \mathrm{VSE}(n) = -\sum_{q=1}^{N} \beta_q = -(4\beta + 4\beta') = -8\beta = 8|\beta|$.

The intermediate curve in Figure 17(a) corresponds to $\beta' = 0.5\beta$. Its asymptotic limit, $6|\beta|$, is—again—equal to the absolute sum of all bond integrals assigned to an internal monomer:

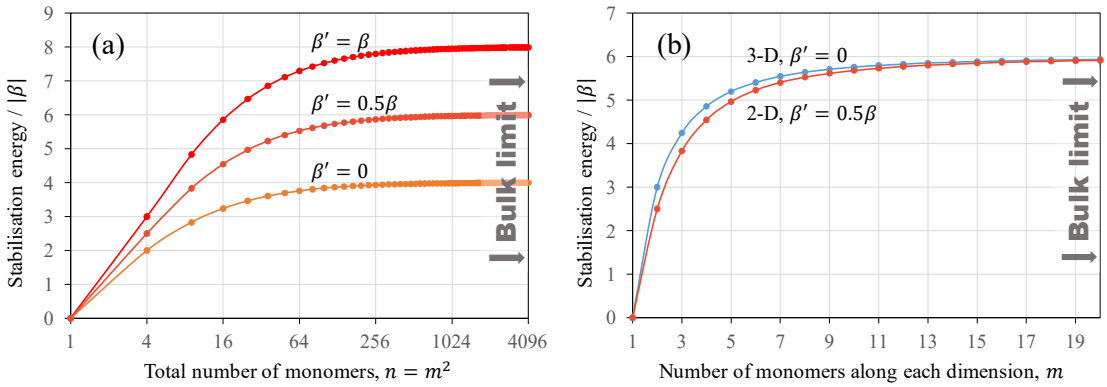

Figure 17. (a) Vertical stabilisation energies (VSE) for the 2-D array from Figure 16 plotted versus the array size, $n = m^2$, on the $\log_2 n$ scale. The three curves shown correspond to $\beta' = 0$, $\beta' = 0.5\beta$, and $\beta' = \beta$, as indicated. (b) Orange: the VSE curve corresponding to the 2-D array from Figure 16, with $\beta' = 0.5\beta$. Plotted on the linear m scale using the corresponding data from (a). Blue: the VSE curve for the 3-D cubic array with nearest-neighbour interactions only, reproduced from Figure 12(b).

$\lim_{n\to\infty} \mathrm{VSE}(n) = -\sum_{q=1}^{N} \beta_q = -(4\beta + 4\beta') = -6\beta = 6|\beta|$. Not only is this result in agreement with Equation (22), it also reveals a parallel between this particular 2-D case and the 3-D model accounting for the nearest-neighbour interactions only (Section 4.2.4). Both cases involve 6 units of $|\beta|$ per internal monomer and both approach the same bulk-limit asymptotes.

This prompts the question if the similarity is only found in the asymptotic limit or it applies to the complete stabilisation trends. The answer is in Figure 17(b), which shows two VSE(m) curves. The orange curve corresponds to the 2-D case with $\beta' = 0.5\beta$; it is plotted using the data from Figure 17(a). The blue curve is for the 3-D case, reproduced from Figure 12(b). Although the asymptotic limits are the same, the curves are not identical. This is because the 2-D and 3-D geometric structures are not identical, which does matter for finite arrays.

The overarching summary of the stabilisation trends and an ultimate result of all the model arrays considered in Section 4.2 is expressed by the following general relationship:

$$\mathrm{VSE} = -\sum_{i\neq j} c_i^* c_j \beta_{ij} \tag{23}$$

Here, β_{ij} are the bond integrals for all monomer pairs (not necessarily neighbours), and c_i, $i = 1\ldots n$ are the components of the normalised eigenvector describing the lowest-energy IMO, $\phi_1 = \sum c_i \psi_{\mathrm{LVO}}^{(i)}$. Equation (23) describes any cluster bound by the sharing of one excess electron among n closed-shell monomers. It concisely states that the overall stabilisation energy of such a cluster is the sum of all IM interactions (β_{ij}), weighted by the Hückel-style bond orders, $c_i^* c_j$. (These are the bond orders defined in the Hückel theory [100], as opposed to the nominal bond orders in Lewis structures—the two are not the same.)

The above conclusion crystallizes an intuitive insight, but Equation (23) should not be regarded as a count of the IM bonds in a given cluster. The double-sum in the equation is with respect to pairs of the $\psi_{\mathrm{LVO}}^{(i)}$ basis functions or, equivalently, the $\mathrm{X}^{(i)}$ monomers, rather than the $\mathrm{X}^{(i)}$–$\mathrm{X}^{(j)}$ bonds. This means that each $\mathrm{X}^{(i)}$– $\mathrm{X}^{(j)}$ bond integral contributes to the equation twice: once as β_{ij} and once as β_{ji}. For the sake of a simple illustration, consider—again—an X_2^- dimer anion, $[\mathrm{X}^{(1)}\text{–}\mathrm{X}^{(2)}]^-$, such as $(\mathrm{CO}_2)_2^-$. Its Hückel-style treatment was given in Section 4.2.1. We have: $\beta_{12} = \beta_{21} = \beta_{1/2}$ and the normalised eigenvector defining the bonding IMO is $(c_1, c_2) = \left(1/\sqrt{2}, 1/\sqrt{2}\right)$. With that, the explicit application of Equation (23) is as follows:

$$\mathrm{VSE}(\mathrm{X}_2^-) = -(c_1^* c_2 \beta_{12} + c_2^* c_1 \beta_{21}) = -\left(\tfrac{1}{\sqrt{2}}\tfrac{1}{\sqrt{2}}\beta_{1/2} + \tfrac{1}{\sqrt{2}}\tfrac{1}{\sqrt{2}}\beta_{1/2}\right) = -\beta_{1/2} \tag{24}$$

This agrees with the result from Section 4.2.1. If we counted bonds—in X_2^- there is only one—instead of the monomers, there would be only one term in the parentheses in Equation (24) and the result would be only-half of the correct value.

Similarly, for the triple-decker anion $[\mathrm{X}^{(1)}\text{–}\mathrm{X}^{(2)}\text{–}\mathrm{X}^{(3)}]^-$ from Section 4.2.2 (the model for the biacetyl trimer), we assumed that $\beta_{12} = \beta_{21} = \beta_{23} = \beta_{32} = \beta_{1/4}$ and $\beta_{13} = \beta_{31} = 0$. The corresponding lowest-energy eigenvector is $(1/2,\ 1/\sqrt{2},\ 1/2)$. Equation (23) then yields:

$$\begin{aligned}\mathrm{VSE}(\mathrm{X}_3^-) &= -(c_1^* c_2 \beta_{12} + c_2^* c_1 \beta_{21} + c_1^* c_3 \beta_{13} + c_3^* c_1 \beta_{31} + c_2^* c_3 \beta_{23} + c_3^* c_2 \beta_{32}) \\ &= -\left(\tfrac{1}{2}\tfrac{1}{\sqrt{2}}\beta_{1/4} + \tfrac{1}{\sqrt{2}}\tfrac{1}{2}\beta_{1/4} + \tfrac{1}{2}\tfrac{1}{2}0 + \tfrac{1}{2}\tfrac{1}{2}0 + \tfrac{1}{\sqrt{2}}\tfrac{1}{2}\beta_{1/4} + \tfrac{1}{2}\tfrac{1}{\sqrt{2}}\beta_{1/4}\right) = -\sqrt{2}\beta_{1/4},\end{aligned} \tag{25}$$

in agreement with the result from Section 4.2.2.

A particularly compelling case for the utility of Equation (23) can be made in special cases, when diagonalising the Hamiltonian matrix is either impractical or undesirable for pedagogical reasons. For one example, we turn back to the cubic structure in Figure 15. In Section 4.2.4, Equation (19), we expressed its explicit 8×8 Hamiltonian matrix, which may be too cumbersome to solve on paper. If one looks for a computer-free insight, Equation (23) provides a means of determining the stability of this system, which avoids explicitly solving the 8×8 eigenvalue problem. It is obvious (by symmetry) that the lowest-energy eigenvector must consist of 8 equal c_i, $i = 1 \ldots 8$, coefficients, because all 8 corners of the cube are equivalent and the ground state must not have nodes. Combining this knowledge with the normalisation requirement, the coefficients are easily determined to be $c_i = 1/\sqrt{8}$. The stabilisation energy is then calculated directly from Equation (23), without solving for all eigenvalues:

$$\mathrm{VSE}(X_8^-) = -\sum_{i=1}^{8}\sum_{\substack{j=1\\ j\neq i}}^{8} c_i^* c_j \beta_{ij} = -8 \times 3 \times \frac{1}{\sqrt{8}}\frac{1}{\sqrt{8}}\beta = -3\beta \qquad (26)$$

The 8×3 factor replacing the above double-sum accounts for 8 monomers, each connected to three other monomers (Figure 15) by bond integrals β. All other bond integrals, i.e., those between the opposite corners of the cube and between the opposite corners of each side of the cube, are set to zero, as was assumed in Section 4.2.4. The result of the one-line calculation in Equation (26), VSE = -3β, is identical to that in Section 4.2.4, where it was determined numerically using a direct diagonalisation procedure.

Unlike Equation (22), Equation (23) allows one to evaluate the covalent stabilisation energy of any type-I cluster, large or small. Equation (22) is an asymptotic expression describing the "bulk" limit of large clusters, but Equation (23) holds for any size. Furthermore, it does not rely on the definition of an "internal" monomer, in the way Equation (22) does. In fact, in the above 2×2×2 example, all monomers belong to the cluster boundary, i.e., none are internal. The general nature of Equation (23) also yields insight into the size- and geometry-dependent cluster stabilities, including both the intermediate and bulk-limit behaviours of the stabilisation curves. It allows to distinguish the contributions of the internal part of the system from those of its boundary. It makes it clear why in the asymptotic limit the cluster stability converges on the bonding stabilisation of a single, arbitrarily chosen "internal" monomer. Indeed, the sum in Equation (23) can be partitioned into the contributions of the internal and boundary monomers. As the cluster size increases, the internal mole fraction approaches 1, and in the asymptotic limit the sum in Equation (23) becomes the averaged property of a single internal monomer.

The existence of asymptotic limits for all stabilisation curves in Figures 12 and 17 indicates that the bonding power of one electron in any cluster is (unsurprisingly) finite. However, the variation of the asymptotic values, summarised in Equation (22), proves that the cluster stability depends on the bonding connectivity of the monomers. That can be helped by increasing the number of spatial dimensions but in the end, it is the combined energy of all bonds formed by a monomer that matters, not the system's dimensionality. For this reason, any geometric or other constraints hindering the formation of covalent bonds within a cluster may have an adverse effect on its stability. The overarching message is that the bonding power of an electron is not its own intrinsic property but a result of interaction with the cooperative network of cluster building blocks, as described by the IMO formalism and Equation (23).

5. General factors controlling type-I cluster anion structures

Many known cluster anion families exhibit the coexistence or competition of different core anion types. The extensively studied [7,8,10-12,22,65] $(CO_2)_n^-$ clusters have covalent dimer-anion [9] cores in the range $n = 2–6$ and $n > 13$ and the monomer anion cores in the intermediate size range [7,8]. Remarkably, none of the $(CO_2)_n^-$ clusters are known to have trimer or larger polymer anion cores, although plausible geometries for them can be envisaged. In general, core-size limits are common among type-I cluster anions.

Using the model findings from Section 4, we can now consider two factors that hinder anionic charge-sharing polymerisation in type-I systems, typically limiting the size of cluster cores to dimer or, in rare cases, trimer anions. The first factor is the dependence of IM bond integrals on the cluster geometry. The second is the sometimes-counterintuitive energetics of the competition between the covalent and solvation forces.

5.1. *Geometric constraints on covalent bonding*

We first illustrate the role of geometric constraints on IM covalent bonding using the example of $(CO_2)_n^-$, before proceeding to a more general discussion. As in the general MO theory, for an IMO to form, the monomer LVOs must effectively overlap. We glossed over this requirement in Section 4 but will now consider its ramifications.

A linear CO_2 monomer does not bind an electron. Although intense debate about the nature of the temporary CO_2^- anion continues to this day (the reader is referred to References [112-114] and the articles cited therein), historically CO_2^- has been viewed as a bent, short-lived structure, which is only vertically (not adiabatically) bound [115,116]. There is recent theoretical evidence that this textbook picture is incorrect, and the short-lived anion of CO_2 is in fact a non-valence correlation-bound species [114]. Even so, the valence anion is likely to emerge in the presence of stabilising interactions in clusters, which favour a more localised charge. The bent geometry of valence CO_2^- is dictated by the corresponding LVO, sketched in Figure 2. Any CO_2 moiety bearing even partial negative charge is expected to have a bent structure. Past studies of halide anions solvated by CO_2 established a correlation between the OCO bond angle and partial charge sharing in these systems [117-120].

The structure of the CO_2 dimer anion, which can be described as $^{-1/2}O_2C–CO_2^{-1/2}$, is easily understood in this framework: it results from heads-on coupling of two partially charged and, therefore, bent $CO_2^{-1/2}$ moieties, as illustrated by the diagram in Figure 2. The resulting D_{2d} symmetry structure, first predicted by Fleischman and Jordan [9], is shown in Figure 18(a), along with the IMO responsible for the IM half-bond. In the CMMO model, the IMO is described as a superposition of the LVOs belonging to the two monomers, according to Equation (3). The general treatment of such type-I dimer anions in Section 4.2.1 yielded a VSE = $-\beta_{1/2}$.

The IM bonding and charge sharing make the dimer more robust than the monomer anion. The covalent dimer is stable with respect to dissociation and electron detachment, and more stable than $CO_2^-\cdot CO_2$ [9]. While the triumph of covalent stabilisation in $(CO_2)_2^-$ is not surprising, it does not extend to larger $(CO_2)_n^-$ clusters. For example, the addition of a third monomer to $(CO_2)_2^-$ does not yield a covalent trimer anion, $(CO_2)_3^-$. In fact, none of the $(CO_2)_n^-$ clusters are known to have covalently bound trimer- or larger polymer-anion cores. The reason, as already noted, is twofold, but we turn to the geometric hinderance first.

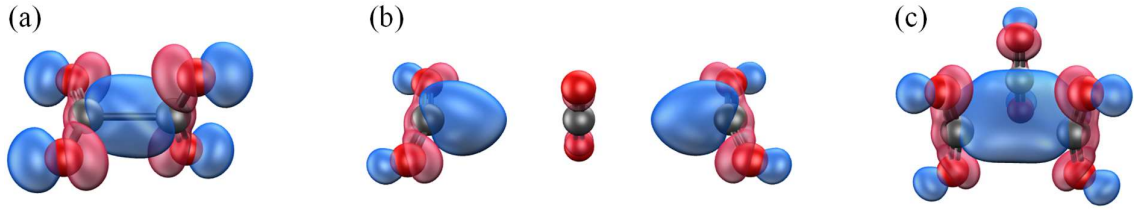

Figure 18. (a) The D_{2d} symmetry $(CO_2)_2^-$ structure, plotted along with the IMO responsible for the IM half-bond. (b) An unbound D_{2h} symmetry $(CO_2)_3^-$ chain structure, described as $^{-1/2}(CO_2)$-(CO_2)-$(CO_2)^{-1/2}$, with its IMO. (c) An unbound D_{3h} symmetry $(CO_2)_3^-$ structure with three equivalent IM bonds and equal charge sharing between the monomers.

The geometric constraints come into play in many systems when one attempts to extend covalent bonding to species larger than a dimer. The reason is simple: effective overlap of more than two MMOs is harder to achieve. In the case of CO_2, the mono-directional geometries of a bent monomer and its LVO make it implausible for the $(CO_2)_3^-$ trimer anion to adopt a chain structure similar to the biacetyl trimer anion in Figure 3(c). Chain trimer anions follow the $[X\text{-}X\text{-}X]^-$ triple-decker motif examined in Section 4.2.2. In it, the middle monomer bonds to two, not one, neighbours. In the case of X = CO_2, this would require the middle CO_2 to adopt a bidirectional linear geometry, which is not conducive to charge sharing.

To develop this example in some detail, a $(CO_2)_3^-$ chain structure is shown in Figure 18(b). We attempted to optimise it subject to the D_{2h} symmetry constraint, using the B3LYP density functional with the aug-cc-pVDZ basis set in QChem 5.1 [121]. The resulting lowest-energy IMO, included in the figure, is only nominally bonding. The $\psi_{\mathrm{LVO}}^{(2)}$ contribution to the ϕ_1 IMO is non-existent and hence the overall orbital has a non-bonding IM character. Not surprisingly, this $^{-1/2}(CO_2)$-(CO_2)-$(CO_2)^{-1/2}$ structure is unbound.

A $(CO_2)_3^-$ bonding motif that is a better fit to the CO_2 LVO properties is shown in Figure 18(c). The D_{3h} symmetry trimer corresponds to the generic triangular X_3^- structure with three equivalent order-of-1/6 IM bonds and equal charge sharing between the monomers. Its Hückel-style treatment at the end of Section 4.2.2 yielded a VSE = $-2\beta_{1/6}$. Although the structure in Figure 18(c) may look reminiscent of the recently reported trimer of carbon monoxide [107], the latter is a type-III, not type-I, anion. As discussed in Section 3.2.3, the IM bonding in type-III species is more robust and more complex than in type-I clusters. Because of this, the similarity between the $(CO)_3^-$ and $(CO_2)_3^-$ triangular structures is superficial. The $(CO_2)_3^-$ triangular structure in Figure 18(c) is only about 0.2 eV (according to B3LYP/aug-cc-pVDZ) more stable than its chain counterpart in Figure 18(b), and it is not a true potential minimum. It is unstable with respect to dissociation and less stable than $(CO_2)_2^-{\cdot}CO_2$. In support of these conclusions, all experimental evidence shows that CO_2 cluster anions have either covalent dimer or monomer anion cores, never trimers or beyond [7,8,65,122-126].

More generally, we have already noted in Section 4.2 that the bond integrals for IM interactions depend on the MMO overlap and, therefore, the bond geometry. That includes not only the bond length, but also the relative orientation of the MMOs. Figure 19 illustrates in sketch form the overlap of the main carbon lobes of the monomer LVOs in (a) $(CO_2)_2^-$ and (b) triangular $(CO_2)_3^-$. Neglecting the reality of different bond orders (1/2 vs. 1/6), both stetches assume the same C–C bond distances. Even so, due to the different angles between the overlapping MMO axes (180° in (a) vs. 120° in (b)), the MMO overlap in the triangular trimer (b) is smaller

Figure 19. Overlap of the carbon lobes of the monomer LVOs in (a) $(CO_2)_2^-$ and (b) triangular $(CO_2)_3^-$.

than in the dimer (a). That is, even under the assumption of equal bond lengths, we should expect the bond integral in (b) to be smaller in magnitude than the corresponding integral in (a). The difference in bond orders enhances this effect further.

These geometry considerations are part of the general symmetry requirement for forming MOs or IMOs. In the discussion of various arrays in Section 4, it was assumed implicitly that the $\psi_{\mathrm{LVO}}^{(i)}$ basis functions from different monomers have correct symmetry properties to interact with their neighbours. This requirement is always satisfied for *s* type atomic MMOs but presents challenges in other cases. For example, the π types LVOs of organics are prone to forming stacked π-π bonded arrays [39,40,66-68,106], which assemble along one dimension only. In general, the interacting MMO symmetry must be considered for each specific system.

5.2. *Effects of solvation on covalent bonding*

We already established that individual IM bonds weaken rapidly as the size of a type-I anion is increased. In addition to the bond lengths generally increasing with decreasing nominal bond order, other types of geometric limitations may come into play in clusters larger than a dimer. These factors may either prevent the very possibility of IM bond formation or further decrease the magnitudes of the bond integrals, as illustrated by the example in Figure 19. As the IM covalent bonds weaken, additional competition in larger clusters comes from solvation, which generally favours core anions of smaller size.

In this section, we integrate the CMMO treatment of covalent and solvation interactions into a unified model, which includes both electrostatic and charge-sharing terms. The basic elements of the model are developed in Section 4. Now, we turn to the general description of a homogeneous cluster anion X_n^- with a covalently bound core of size k, solvated by $(n-k)$ neutral monomers, i.e., $X_k^-{\cdot}X_{n-k}$. The formalism for describing the covalent core structure was presented in Section 4.2, while the solvation interactions were addressed in Section 4.1. Here, we combine the two types of interactions into one practical theory.

To simplify the description, we will replace the individual solvation factors σ_i introduced in Section 4.1 with the average quantities $\sigma_{k,n-k}$, which describe the total stabilisation of the X_k^- core anion by solvation with $(n-k)$ neutral monomers. Just like the individual factors σ_i in Equation (10), $\sigma_{k,n-k}$ are defined as negative quantities, reflecting the stabilising nature of the interactions. In the case of a monomer-anion cluster core, i.e., for a cluster described as $X^-{\cdot}X_{n-1}$, all individual σ_i in Equation (10) are replaced by the same average quantity $\sigma_{1,n-1}$. Furthermore, the Coulomb integrals α_i are identical for all monomers in a homogeneous cluster. We set all $\alpha_i = \alpha$ and Equation (10) simplifies to:

$$\mathbf{H} = \begin{pmatrix} \alpha+\sigma_{1,n-1} & 0 & \cdots & 0 \\ 0 & \alpha+\sigma_{1,n-1} & \cdots & 0 \\ \vdots & \vdots & \ddots & \vdots \\ 0 & 0 & \cdots & \alpha+\sigma_{1,n-1} \end{pmatrix} \tag{27}$$

Each diagonal element H_{ii} in Equation (27) describes the effect of placing the excess electron on the corresponding monomer, $X^{(i)}$. For an arbitrary $X_k^-{\cdot}X_{n-k}$ cluster, we have a covalently bound core and $(n-k)$ remaining monomers not involved in covalent IM bonding. The Hückel-style Hamiltonian matrix for such system assumes a block-diagonal form, with each block describing the placement of the excess electron on the corresponding monomer or monomer group. For $X_k^-{\cdot}X_{n-k}$, there is a $k \times k$ block describing the X_k^- cluster core (per Section 4.2), with the additional stabilisation $\sigma_{k,n-k}$ included in this block's diagonal elements to account for the solvation of the core anion by $(n-k)$ neutral monomers (per Section 4.1). The remaining blocks all consist of single diagonal elements only, each describing the solvation of a monomer anion by $(n-1)$ neutral monomers, just like in Equation (27), i.e., $\sigma_{1,n-1}$.

For example, the matrix

$$\mathbf{H} = \begin{pmatrix} \alpha + \sigma_{2,1} & \beta_{1/2} & 0 \\ \beta_{1/2} & \alpha + \sigma_{2,1} & 0 \\ 0 & 0 & \alpha + \sigma_{1,2} \end{pmatrix} \tag{28}$$

describes an $X_2^-{\cdot}X$ cluster anion. The first 2×2 block represents the covalently bound dimer, which, by itself, would be described by Equation (13). In $X_2^-{\cdot}X$, the dimer anion is additionally solvated by one neutral X moiety, and this is described by the $\sigma_{2,1}$ solvation factors added to the diagonal elements of the 2×2 block. The second block, comprised of a single element $\alpha + \sigma_{1,2}$, represents the placement of the charge on the third monomer, i.e., an X^- moiety, not participating in IM bonding, but stabilised by two solvent monomers ($\sigma_{1,2}$). The first two eigenvalues of Equation (28), $E_{1,2} = \alpha \pm \beta_{1/2} + \sigma_{2,1}$, describe the target $X_2^-{\cdot}X$ structure, in which the charge is shared between the two X moieties of the core anion ('+' before the bond integral corresponds to an order-of-1/2 IM bond, '–' to an anti-bond). The third eigenvalue, $E_3 = \alpha + \sigma_{1,2}$, describes an $X_2{\cdot}X^-$ cluster, with the charge localised on one X moiety. Importantly, the solvation factors are not the same within the two blocks: $\sigma_{2,1}$ represents the stabilisation of X_2^- by one neutral X, while $\sigma_{1,2}$ describes the solvation of X^- by two neutral X moieties. Based on the arguments presented below, we expect $|\sigma_{2,1}| < |\sigma_{1,2}|$. This expectation is part of the general trends for the solvation factors. Using the extensive knowledge of the energetics of various cluster systems [3,5,40], these trends can be summarised as follows.

First, for a given core size k, we expect $\sigma_{k,n-k}$ to increase in magnitude with increasing number of solvating monomers, $(n-k)$, because the more solvent monomers interact with the same core anion, the greater the overall stabilisation effect. However, the gradual increase in $|\sigma_{k,n-k}|$ due to stepwise solvation is slower than linear: for large clusters, we expect the overall solvation of the core anion to reach the bulk limit. That is, while in general

$$|\sigma_{k,1}| < |\sigma_{k,2}| < |\sigma_{k,3}| < \dots \tag{29}$$

we also expect

$$|\sigma_{k,1}| > |\sigma_{k,2} - \sigma_{k,1}| > |\sigma_{k,3} - \sigma_{k,2}| > \dots \tag{30}$$

On the other hand, at least for clusters within the first solvation shell, increasing the core size k while keeping the number of solvent monomers $(n-k)$ constant generally leads to a

decrease in the solvation energy:

$$\left|\sigma_{1,n-k}\right| > \left|\sigma_{2,n-k}\right| > \left|\sigma_{3,n-k}\right| > \cdots \tag{31}$$

This is because of the decrease in charge density with increasing core anion size. For example, in solvation by a single neutral monomer, the monomer anion is stabilised more significantly than its dimer- or trimer-anion counterparts: $|\sigma_{1,1}| > \left|\sigma_{2,1}\right| > \left|\sigma_{3,1}\right|$.

In the case of $X_2^-{\cdot}X$, the energetic ordering of the eigenvalues for Equation (28) depends on the relative magnitudes of the IM bond integral $\beta_{1/2}$ and the solvation differential $(\sigma_{1,2} - \sigma_{2,1})$. If $|\beta_{1/2}| > |\sigma_{1,2} - \sigma_{2,1}|$, then E_1 is the lowest eigenvalue and the $X_2^-{\cdot}X$ structure is preferred, with VSE = $-(\beta_{1/2} + \sigma_{2,1})$. If the covalent bonding is weaker than the solvation differential, E_3 is the lowest eigenvalue and it is more favourable for the charge to localise of one monomer, rather than form a bond between two. The cluster then adopts the $X_2{\cdot}X^-$ (or $X^-{\cdot}X_2$) configuration with VSE = $-\sigma_{1,2}$.

As a slightly more complex example, we will consider a covalently bound triple-decker anion solvated by two additional neutral monomers: $X_3^-{\cdot}X_2$ (n = 5, k = 3). It is described by the CMMO matrix:

$$\mathbf{H} = \begin{pmatrix} \alpha + \sigma_{3,2} & \beta_{1/4} & 0 & 0 & 0 \\ \beta_{1/4} & \alpha + \sigma_{3,2} & \beta_{1/4} & 0 & 0 \\ 0 & \beta_{1/4} & \alpha + \sigma_{3,2} & 0 & 0 \\ 0 & 0 & 0 & \alpha + \sigma_{1,4} & 0 \\ 0 & 0 & 0 & 0 & \alpha + \sigma_{1,4} \end{pmatrix} \tag{32}$$

The leading 3×3 block corresponds to the $[X\text{-}X\text{-}X]^-$ triple-decker structure, which by itself would be described by Equation (14). In Equation (32), the added solvation factors $\sigma_{3,2}$ within the triple-decker block describe the stabilisation of the trimer-anion core by two neutral monomers. The single-element blocks on the main diagonal in Equation (32), H_{44} and H_{55}, are both equal to $(\alpha + \sigma_{1,4})$. The each correspond to the excess electron being placed on a single monomer solvated by four neutrals.

The first three eigenvalues of Equation (32), $E_1 = \alpha + \sqrt{2}\beta_{1/4} + \sigma_{3,2}$, $E_2 = \alpha + \sigma_{3,2}$, and $E_3 = \alpha - \sqrt{2}\beta_{1/4} + \sigma_{3,2}$, describe the $X_3^-{\cdot}X_2$ structure. E_1 corresponds to the covalently bound triple-decker cluster core with VSE = $-(\sqrt{2}\beta_{1/4} + \sigma_{3,2})$, while E_2 and E_3 describe the excess electron entering the nonbonding and antibonding trimer IMOs, respectively. The other two degenerate eigenvalues, $E_{4,5} = \alpha + \sigma_{1,4}$, correspond to the $X^-{\cdot}X_4$ structure with VSE = $-\sigma_{1,4}$. As in the previous example, the character of the most stable structure depends on the relative magnitudes of the bond integrals and solvation differentials.

5.3. *Solvation hinders type-I polymerisation*

The presented formalism gives a bird's eye description of IM covalent and solvation interactions in cluster anions. While not precise, it offers an appealing advantage over full-scale calculations in providing a simple picture of the forces controlling cluster properties.

As described so far, the model has assumed either purely covalent or purely electrostatic interactions between pairs or groups of monomers. To quantify its performance, the CMMO

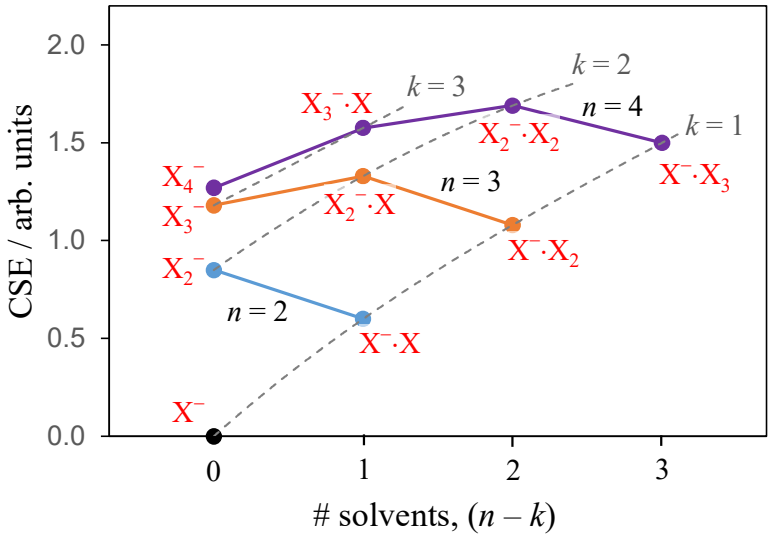

Figure 20. Cluster stabilisation trends for $X_k^-{\cdot}X_{n-k}$ clusters, predicted by the CMMO model. The CSE values are plotted versus the number of neutral solvent monomers, $(n - k)$, in each cluster. Solid lines for $n = 2 - 4$ represent trendlines for clusters of the same size (n = const), but with varying sizes of the core anion (k). Dashed lines $k = 1 - 3$ follow stepwise solvation trends for a given core anion.

predictions were previously compared to the properties of various known clusters, including the π-π bonded clusters of glyoxal and biacetyl [40]. The comparisons were used to quantify the model parameters and assess the IM bonding characters in specific systems. One particularly instructive outcome of this analysis is shown in Figure 20. It displays the predicted stabilisation trends for generic $X_k^-{\cdot}X_{n-k}$ clusters structures with n = 1–4 [40]. The stabilisation energies predicted by the CMMO model are plotted versus the number of solvent monomers $(n - k)$. The structural formulas are indicated next to each data symbol.

Several points should be mentioned before discussing the results. First, the sample calculations do not account for mixed covalent and electrostatic interactions within a cluster core. The mixing is discussed in Section 5.4 in connection with resonance structures. The results presented here should be viewed as basic cluster types, subject to quantum superpositions. Second, Figure 20 is intended to be generic, applicable to diverse cluster families. For this reason, the stabilisation energies are expressed in arbitrary units, intended to correspond only approximately to electron-volts. The key information in the figure is unit independent, revealed by the general trend rather than specific values. Third, for the X_k^- cluster cores larger than a dimer, linear-chain (stacked) structures were assumed in the analysis. Fourth, the stabilisation energies in Figure 20 correspond to overall cluster stabilisation energies (CSE), which differ from the vertical (VSE) quantities by the inclusion of the monomer relaxation energy, ΔE_{rel}:

$$\mathrm{CSE} = \mathrm{VSE} - \Delta E_{rel} \tag{33}$$

The VSE quantities were determined using the unified CMMO formalism described in Section 5.2. The reader is referred to Reference [40] for further details, including the ΔE_{rel} values.

Based on the four $(n - k) = 0$ data points in Figure 20, the initial increase in CSE versus n for the purely covalent X_n^- structures saturates quickly. This observation highlights the findings for the linear chain arrays in Section 4.2.4 and the quantitative results for 1-D arrays in Figure 12. Next, to help identify the general trends, two types of trend lines are included in Figure 20.

The solid lines connect the data points for clusters of the same size (n = const), but with varying sizes of the core anions (k), e.g. X_3^-, $X_2^-\cdot X$, and $X^-\cdot X_2$. The dashed lines represent stepwise solvation of a given core anion (k = const), e.g. X^-, $X^-\cdot X$, $X^-\cdot X_2$, and $X^-\cdot X_3$. The maximum of each solid curve represents the most stable cluster structure for that size n.

The key result is that for all three solid curves in the figure, the largest-CSE data point falls on the k = 2 dashed trendline. That is, for each of the n = 2, 3, and 4 clusters, the most stable structure corresponds to a covalently bound dimer-anion cluster core, solvated by the remaining X moieties: X_2^-, $X_2^-\cdot X$, and $X_2^-\cdot X_2$, respectively. We conclude that among the covalent cores of all possible sizes, the dimer anion is most favoured, under the assumptions made in the calculations [40]. Although departures from the dimer-only rule are possible, the overall trend holds: solvation generally hinders type-I anionic polymerisation beyond the dimer.

The underlying reason was discussed in Section 4.2. In type-I systems, charge-sharing polymerisation spreads the limited (order-of-1/2) bonding power of one polymerising electron among several ($k - 1$, in the X_k^- chain-anion case) IM bonds. Not only does each bond average a nominal bond order of merely $\frac{1}{2(k-1)}$, but the corresponding bond integrals also decrease in magnitude (Section 4.2.2), weakening the bonding further. The polymerisation process can, therefore, be easily hindered by solvation interactions or vibronic couplings. In the context of the CMMO model, the formation of type-I trimers and beyond requires particularly favorable MMO overlap, as in the π-stacked trimer anions of tetrachloroquinone [106] and biacetyl [68]. Overall, however, the trend observed in Figure 20 predicts that type-I trimer- (and larger) anion cores should be uncommon in cluster studies. And indeed they are.

5.4. *Mixed-character interactions*

The specific CMMO solutions discussed so far assume either covalent (described by bond integrals β_{BO}) or electrostatic (described by solvation factors $\sigma_{k,n-k}$) interactions between pairs or groups of monomers. The clusters described by the Hückel-style Hamiltonian matrices in Equations (13)–(19) are specific cases of purely covalent IM interactions. The diagonal matrices in Equations (8)–(12) and (27) correspond to purely solvated systems with monomer-anion cores (no covalent IM interactions). In contrast, the unified formalism in Section 5.2 includes both covalent and electrostatic IM interactions. For example, Equation (28) describes a cluster comprised of a covalently bound dimer-anion core, electrostatically solvated by one additional neutral monomer. Similarly, Equation (32) describes a trimer-anion core solvated by two neutral monomers. Even though the last two examples involve both covalent and electrostatic forces within the same cluster, the two types of interactions are not mixed in the quantum sense. Each individual interaction is still assumed to be either purely covalent or purely electrostatic in nature and no charge delocalisation from the core anion to the nearest solvents is permitted.

Real clusters may involve admixtures of this basic bonding types. The following examples illustrate the mixed-interactions picture and provide a roadmap for resolving it. To define the problem, we first consider the general case of mixed covalent and electrostatic interactions in a generic $[X\cdot Y]^-$ cluster, where X and Y are not necessarily the same. Without any IM interactions, the $(X + Y)^-$ system is described by Equation (8). As discussed in Section 4.1, this non-interacting system resolves to two possible eigenstates, $(X^- + Y)$ and $(X + Y^-)$.

It may be tempting to include both electrostatic and covalent interactions between the X and Y monomers into one interaction matrix:

$$\mathbf{H_{int}} = \begin{pmatrix} \sigma_{X^-\cdot Y} & \beta \\ \beta & \sigma_{X\cdot Y^-} \end{pmatrix} \tag{34}$$

Combined with **H** from Equation (8), $\mathbf{H_{int}}$ gives a seemingly complete description of $[X\cdot Y]^-$. However, this argument is significantly flawed. The solvation factors in Equation (34) are defined under the assumption of complete charge localisation on either X (for $\sigma_{X^-\cdot Y}$) or Y (for $\sigma_{X\cdot Y^-}$). That is, they are defined for the unmixed eigenstates of Equation (8) or, equivalently, Equation (9). These states are not eigenstates of Equation (34), if $\beta \neq 0$. This means that the $\sigma_{X^-\cdot Y}$ and $\sigma_{X\cdot Y^-}$ factors appearing in the eigenvectors and eigenenergies for combined Equations (8) and (34) are generally incorrect. As written, the $\mathbf{H} + \mathbf{H_{int}}$ Hamiltonian depends explicitly on the properties of its own eigenstates, creating a circular problem. We can obtain approximate solutions in two opposite regimes: $|\beta| << |\sigma_{X^-\cdot Y}|, |\sigma_{X\cdot Y^-}|$ and $|\beta| >> |\sigma_{X^-\cdot Y}|, |\sigma_{X\cdot Y^-}|$.

The first regime corresponds to a weak IM covalent coupling, which can be treated as a first-order perturbation of the ion-molecule complex $X^-\cdot Y$. It applies, for example, to a halide anion (X = I, Br, or Cl) solvated by carbon dioxide ($Y = CO_2$) [117-120]. Section 4.1 outlined the basic zeroth-order model for such clusters, assuming 100% charge localisation on the halide, as in the first eigenstate of Equation (9). Real halide-CO_2 clusters involve a degree of mixing of the electrostatic and covalent interactions. For example, the photoelectron spectra of $Cl^-\cdot CO_2$ indicate a 3.5-7% charge transfer to CO_2 [118], which is a signature of a covalent contribution to the primarily electrostatic interaction. The effect is less significant in $I^-\cdot CO_2$ [117] and $Br^-\cdot CO_2$, but much greater in $F^-\cdot CO_2$ [118], which should be more appropriately described as an FCO_2^- molecular ion rather than an ion-molecule complex [127-129].

To account for the slight covalent character of the predominantly electrostatic interaction in species like $I^-\cdot CO_2$, $Br^-\cdot CO_2$, $Cl^-\cdot CO_2$, we can partition the interaction Hamiltonian in Equation (34) into the diagonal (electrostatic) and off-diagonal (covalent) terms. The former is to be combined with Equation (8), giving the zeroth-order matrix in Equation (9), which we will now label $\mathbf{H_0}$. It describes the ion-molecule complex with the purely electrostatic $X^-\cdot Y$ and $X\cdot Y^-$ eigenstates illustrated in Figure 9(c) and (d), respectively. The remainder of $\mathbf{H_{int}}$ describes the perturbation ($\mathbf{H'}$) of these eigenstates by weak covalent coupling:

$$\mathbf{H} = \mathbf{H_0} + \mathbf{H'} = \begin{pmatrix} \alpha_X + \sigma_{X^-\cdot Y} & 0 \\ 0 & \alpha_Y + \sigma_{X\cdot Y^-} \end{pmatrix} + \begin{pmatrix} 0 & \beta \\ \beta & 0 \end{pmatrix} \tag{35}$$

The corrections to the zeroth-order eigenstates can now be determined using the first-order perturbation theory, neglecting the effect of the weak covalent coupling on the zeroth-order solvation factors.

The second regime corresponds to strong IM covalent coupling experiencing a slight perturbation from electrostatic forces. In this case, we partition $\mathbf{H_{int}}$ in Equation (34) into the large off-diagonal and small diagonal terms. The former is combined with Equation (8), giving a zeroth-order $\mathbf{H_0}$ matrix similar to Equation (13), with the caveat that if $X \neq Y$, the two Coulomb integrals are distinct. The remainder, containing the solvation factors, is treated as $\mathbf{H'}$:

$$\mathbf{H} = \mathbf{H_0} + \mathbf{H'} = \begin{pmatrix} \alpha_X & \beta \\ \beta & \alpha_Y \end{pmatrix} + \begin{pmatrix} \sigma_{X^-\cdot Y} & 0 \\ 0 & \sigma_{X\cdot Y^-} \end{pmatrix} \tag{36}$$

The $X^-{\cdot}Y$ and $X{\cdot}Y^-$ subscripts in the solvation factors are misleading in this regime. Recall that $\sigma_{X^-\cdot Y}$ and $\sigma_{X\cdot Y^-}$ are determined for the unperturbed zeroth-order eigenstates, which in this regime do not correspond to localised charge distributions. Hence it may be wise to relabel them, for example as σ_1 and σ_2. Since these terms are diagonal, their effect is just to shift the values of the bond integrals. The rest of the solution follows the conventional MO theory.

In the case of a homogeneous cluster (X = Y), $\sigma_1 = \sigma_2$ and the only effect of the solvation perturbation is a shift in the overall energy scale. We can as well absorb the sigmas into the bond integral and treat all interactions together. Thus, in a homogeneous dimer X_2^- there can be no symmetry breaking due to the IM interactions, be they covalent or electrostatic in nature. The covalent $[X\text{-}X]^-$ structure is described by a –0.50/–0.50 charge distribution, while in the electrostatically solvated $X^-{\cdot}X$ structure the charge is localised on one monomer. However, in the absence of external perturbations, the $X^-{\cdot}X$ and $X{\cdot}X^-$ structures are strictly degenerate, and the cluster must be described as an $X^-{\cdot}X \leftrightarrow X{\cdot}X^-$ resonance, with the same charge distribution as in the covalent case. In the MO theory, the $[X\text{-}X]^-$ structure itself is a product of electronic coupling between two equivalent $(X^- + X)$ and $(X + X^-)$ structures, which at a closer distance become $X^-{\cdot}X$ and $X{\cdot}X^-$.

The degeneracy of the $(X^- + X)$ and $(X + X^-)$ or $X^-{\cdot}X$ and $X{\cdot}X^-$ structures is easily broken in a larger-cluster environment, or if any asymmetry exists between the two monomers. In the already mentioned dimer anion of biacetyl, $(ba)_2^-$, the there is a slight non-equivalency between the two ba monomers [68], and so this is a good example of a (slightly) heterogeneous $[X\text{-}Y]^-$ cluster. If due to some additional perturbation or couplings, an $[X\text{-}X]^- \leftrightarrow X^-{\cdot}X$ resonance is achieved in a cluster environment, where symmetry can be broken by solvent effects, the resulting structure will also be described by uneven charge sharing.

In the most general sense, therefore, real clusters should be viewed as admixtures of the basic electrostatic and covalent bonding types discussed in this review. We will conclude by illustrating this concept using the π-stacked trimer anion structure of biacetyl, $(ba)_3^-$, shown in Figure 3(c) [68]. Based on density-functional calculations, the $(ba)_3^-$ structure has a –0.17/–0.65/–0.17 Hirshfeld-I charge distribution [40]. This distribution is intermediate between the –0.25/–0.50/–0.25 and 0.00/–1.00/0.00 distributions predicted by the CMMO model for the purely covalent $[X\text{-}X\text{-}X]^-$ and purely electrostatic $X{\cdot}X^-{\cdot}X$ structures, described by Equations (14) and (12), respectively. The actual $(ba)_3^-$ structure results from the $[X\text{-}X\text{-}X]^- \leftrightarrow X{\cdot}X^-{\cdot}X$ resonance, where X = ba. A similar argument also applies to the stacked tetramer-anion of biacetyl, $(ba)_4^-$, whose possible structure is shown in Figure 3(d). As in the trimer case, the charge distribution between the monomers in the computed structure suggests a $[X\text{-}X\text{-}X\text{-}X]^- \leftrightarrow X{\cdot}[X\text{-}X]^-{\cdot}X$ resonance between two unmixed CMMO structures [40].

As a final point concerning the coexistence, competition, and mixing of different cluster structures, the entropic contributions to free energy must also be kept in mind. Entropy favours less-rigid structures and, therefore, smaller-sized covalently bound cluster cores. This creates another hurdle for anionic polymerisation. In cases when the energies of two different cluster isomers are similar, entropy will favour the more solvated form of the cluster with a smaller covalent core. In a similar vein, the limits of electronic coherence due to vibronic couplings in large enough systems also favour charge localisation and smaller-sized cluster cores.

6. Conclusion

We have painted a broad-brush picture of the competing covalent and electrostatic interactions responsible for the structural properties and stability of cluster anions. Our focus was not on the individual chemistry of specific compounds serving as cluster building blocks, but on the cooperative properties of the aggregate molecular networks controlled by a multitude of interactions within them. Treating the monomers as self-contained but interlocking building blocks, we outlined a perspective on the cluster properties derived from the coupled-monomers model. This model relies on the first-order separability of inter- and intra-monomer interactions and offers a description of the inter-monomer covalent bonds in terms of coherent charge sharing. A Hückel-style formalism, adapted specifically to weak covalent and solvation interactions in clusters, offers broad insight into the competition between these types of interactions.

When an electron is added to a network of closed-shell monomers, new covalent bonds may form, resulting in the formation of a dimer or polymer-anion to serve as the cluster core. The IM covalent bonding in such anions is usually weak, because the bonding power of one electron is finite. Moreover, it is not the electron's intrinsic property but a result of interaction within the cooperative network of monomers, as described by the formalism outlined in this review. The formation of weak covalent bonds is subject to the competition from solvation forces. The insight from this work suggests that under typical conditions, the cumulative effect of solvation tends to limit the size of covalently bound cluster cores to monomer, dimer, and, in some cases, trimer anions. The stronger the solvation relative to the covalent forces, the smaller the sizes of the core anions favoured by equilibrium thermodynamics.

Acknowledgements

This work was supported by the U.S. National Science Foundation (grant CHE-1664732).

REFERENCES

[1] A. J. Stone, *The Theory of Intermolecular Forces* 2nd ed. ed. (Oxford University Press, Oxford, 2013).
[2] C. Mackie, A. Zech, and M. Head-Gordon, *J. Phys. Chem. A* **125**, 7750 (2021).
[3] A. W. Castleman and K. H. Bowen, *J. Phys. Chem.* **100**, 12911 (1996).
[4] T. E. Dermota, Q. Zhong, and A. W. Castleman, *Chem. Rev.* **104**, 1861 (2004).
[5] A. Sanov and W. C. Lineberger, *Phys. Chem. Chem. Phys.* **6**, 2018 (2004).
[6] I. Yourshaw, Y. X. Zhao, and D. M. Neumark, *J. Chem. Phys.* **105**, 351 (1996).
[7] M. J. DeLuca, B. Niu, and M. A. Johnson, *J. Chem. Phys.* **88**, 5857 (1988).
[8] T. Tsukuda, M. A. Johnson, and T. Nagata, *Chem. Phys. Lett.* **268**, 429 (1997).
[9] S. H. Fleischman and K. D. Jordan, *J. Phys. Chem.* **91**, 1300 (1987).
[10] M. Saeki, T. Tsukuda, and T. Nagata, *Chem. Phys. Lett.* **348**, 461 (2001).
[11] M. Saeki, T. Tsukuda, and T. Nagata, *Chem. Phys. Lett.* **340**, 376 (2001).
[12] R. Mabbs, E. Surber, L. Velarde, and A. Sanov, *J. Chem. Phys.* **120**, 5148 (2004).
[13] K. M. Ervin and W. C. Lineberger, in *Advances in Gas Phase Ion Chemistry*, edited by N. G. Adams and L. M. Babcock (JAI Press, Greenwich, 1992), Vol. 1 pp. 121-166.
[14] E. R. Grumbling, K. Pichugin, L. Velarde, and A. Sanov, *J. Phys. Chem. A* **114**, 1367 (2010).
[15] T. Kondow and K. Mitsuke, *J. Chem. Phys.* **83**, 2612 (1985).

[16] A. Sanov, S. Nandi, K. D. Jordan, and W. C. Lineberger, *J. Chem. Phys.* **109**, 1264 (1998).
[17] T. Habteyes, L. Velarde, and A. Sanov, *J. Chem. Phys.* **130**, 124301 (2009).
[18] Y. Kobayashi, Y. Inokuchi, and T. Ebata, *J. Chem. Phys.* **128**, 164319 (2008).
[19] T. Habteyes, L. Velarde, and A. Sanov, *J. Phys. Chem. A* **112**, 10134 (2008).
[20] T. Habteyes and A. Sanov, *J. Chem. Phys.* **129**, 244309 (2008).
[21] L. A. Yu, A. H. Zeng, Q. A. Xu, and M. F. Zhou, *J. Phys. Chem. A* **108**, 8264 (2004).
[22] R. Mabbs, E. Surber, and A. Sanov, *Chem. Phys. Lett.* **381**, 479 (2003).
[23] S. Koizumi, H. Yasumatsu, S. Otani, and T. Kondow, *J. Phys. Chem. A* **106**, 267 (2002).
[24] S. W. Zhang, C. G. Zhang, Y. T. Yu, B. Z. Mao, and F. C. He, *Chem. Phys. Lett.* **304**, 265 (1999).
[25] A. Sanov, W. C. Lineberger, and K. D. Jordan, *J. Phys. Chem. A* **102**, 2509 (1998).
[26] T. Maeyama, T. Oikawa, T. Tsumura, and N. Mikami, *J. Chem. Phys.* **108**, 1368 (1998).
[27] T. Tsukuda, T. Hirose, and T. Nagata, *Chem. Phys. Lett.* **279**, 179 (1997).
[28] K. Hiraoka, S. Fujimaki, G. Aruga, and S. Yamabe, *J. Phys. Chem.* **98**, 1802 (1994).
[29] R. J. Li and R. E. Continetti, *J. Phys. Chem. A* **106**, 1183 (2002).
[30] K. Pichugin, E. Grumbling, L. Velarde, and A. Sanov, *J. Chem. Phys.* **129**, 044311 (2008).
[31] L. Velarde, T. Habteyes, E. R. Grumbling, K. Pichugin, and A. Sanov, *J. Chem. Phys.* **127**, 084302 (2007).
[32] T. Tsukuda, M. Saeki, L. Zhu, and T. Nagata, *Chem. Phys. Lett.* **295**, 416 (1998).
[33] L. A. Posey and M. A. Johnson, *J. Chem. Phys.* **88**, 5383 (1988).
[34] J. Hacaloglu, S. Suzer, and L. Andrews, *J. Phys. Chem.* **94**, 1759 (1990).
[35] M. E. Jacox, *J. Chem. Phys.* **93**, 7622 (1990).
[36] M. E. Jacox and W. E. Thompson, *J. Chem. Phys.* **93**, 7609 (1990).
[37] D. W. Arnold and D. M. Neumark, *J. Chem. Phys.* **102**, 7035 (1995).
[38] D. L. Osborn, D. J. Leahy, D. R. Cyr, and D. M. Neumark, *J. Chem. Phys.* **104**, 5026 (1996).
[39] P. A. Pieniazek, A. I. Krylov, and S. E. Bradforth, *J. Chem. Phys.* **127**, 044317 (2007).
[40] Y. Dauletyarov and A. Sanov, *Phys. Chem. Chem. Phys.* **23**, 11596 (2021).
[41] E. J. Hart and J. W. Boag, *J. Am. Chem. Soc.* **84**, 4090 (1962).
[42] M. Armbruster, H. Haberland, and H. G. Schindler, *Phys. Rev. Lett.* **47**, 323 (1981).
[43] J. Schnitker, K. Motakabbir, P. J. Rossky, and R. Friesner, *Phys. Rev. Lett.* **60**, 456 (1988).
[44] L. A. Posey, P. J. Campagnola, M. A. Johnson, G. H. Lee, J. G. Eaton, and K. H. Bowen, *J. Chem. Phys.* **91**, 6536 (1989).
[45] L. A. Posey, M. J. DeLuca, P. J. Campagnola, and M. A. Johnson, *J. Phys. Chem.* **93**, 1178 (1989).
[46] P. J. Campagnola, L. A. Posey, and M. A. Johnson, *J. Chem. Phys.* **92**, 3243 (1990).
[47] J. V. Coe, G. H. Lee, J. G. Eaton, S. T. Arnold, H. W. Sarkas, K. H. Bowen, C. Ludewigt, H. Haberland, and D. R. Worsnop, *J. Chem. Phys.* **92**, 3980 (1990).
[48] S. T. Arnold, R. A. Morris, and A. A. Viggiano, *J. Chem. Phys.* **103**, 9242 (1995).
[49] C. G. Bailey, J. Kim, and M. A. Johnson, *J. Phys. Chem.* **100**, 16782 (1996).
[50] P. Ayotte and M. A. Johnson, *J. Chem. Phys.* **106**, 811 (1997).
[51] J. Kim, I. Becker, O. Cheshnovsky, and M. A. Johnson, *Chem. Phys. Lett.* **297**, 90 (1998).
[52] O. P. Balaj, C. K. Siu, I. Balteanu, M. K. Beyer, and V. E. Bondybey, *Chem-Eur J* **10**, 4822 (2004).
[53] A. E. Bragg, J. R. R. Verlet, A. Kammrath, O. Cheshnovsky, and D. M. Neumark, *Science* **306**, 669 (2004).

[54] K. R. Asmis, G. Santambrogio, J. Zhou, E. Garand, J. Headrick, D. Goebbert, M. A. Johnson, and D. M. Neumark, *J. Chem. Phys.* **126**, 191105 (2007).
[55] K. A. Hanold, C. R. Sherwood, and R. E. Continetti, *J. Chem. Phys.* **103**, 9876 (1995).
[56] K. A. Hanold, M. C. Garner, and R. E. Continetti, *Phys. Rev. Lett.* **77**, 3335 (1996).
[57] H. Hsieh and R. Quirk, *Anionic Polymerization: Principles and practical applications* (Marcel Dekker, New York, 1996).
[58] M. J. DeLuca, C.-C. Han, and M. A. Johnson, *J. Chem. Phys.* **93**, 268 (1990).
[59] C. R. Sherwood, K. A. Hanold, M. C. Garner, K. M. Strong, and R. E. Continetti, *J. Chem. Phys.* **105**, 10803 (1996).
[60] R. J. Li, K. A. Hanold, M. C. Garner, A. K. Luong, and R. E. Continetti, *Faraday Discuss.* **108**, 115 (1997).
[61] A. J. A. Aquino, P. R. Taylor, and S. P. Walch, *J. Chem. Phys.* **114**, 3010 (2001).
[62] D. J. Goebbert and A. Sanov, *J. Chem. Phys.* **131**, 104308 (2009).
[63] D. Khuseynov, D. J. Goebbert, and A. Sanov, *J. Chem. Phys.* **136**, 094312 (2012).
[64] D. Khuseynov, A. R. Dixon, D. J. Dokuchitz, and A. Sanov, *J. Phys. Chem. A* **118**, 4510 (2014).
[65] J. W. Shin, N. I. Hammer, M. A. Johnson, H. Schneider, A. Gloss, and J. M. Weber, *J. Phys. Chem. A* **109**, 3146 (2005).
[66] A. A. Golubeva and A. I. Krylov, *Phys. Chem. Chem. Phys.* **11**, 1303 (2009).
[67] K. B. Bravaya, O. Kostko, M. Ahmed, and A. I. Krylov, *Phys. Chem. Chem. Phys.* **12**, 2292 (2010).
[68] Y. Dauletyarov, A. A. Wallace, C. C. Blackstone, and A. Sanov, *J. Phys. Chem. A* **123**, 4158 (2019).
[69] K. B. Bravaya, B. L. Grigorenko, A. V. Nemukhin, and A. I. Krylov, *Acc. Chem. Res.* **45**, 265 (2012).
[70] C. S. Anstöter, C. R. Dean, and J. R. R. Verlet, *Phys. Chem. Chem. Phys.* **19**, 29772 (2017).
[71] T. Xue, A. R. Dixon, and A. Sanov, *Chem. Phys. Lett.* **660**, 205 (2016).
[72] M. R. Nimlos, G. Davico, C. M. Geise, P. G. Wenthold, W. C. Lineberger, S. J. Blanksby, C. M. Hadad, G. A. Petersson, and G. B. Ellison, *J. Chem. Phys.* **117**, 4323 (2002).
[73] L. Salem and C. Rowland, *Angew. Chem. Int. Ed.* **11**, 92 (1972).
[74] K. A. Hanold and R. E. Continetti, *Chem. Phys.* **239**, 493 (1998).
[75] J. A. Kelley, W. H. Robertson, and M. A. Johnson, *Chem. Phys. Lett.* **362**, 255 (2002).
[76] K. Hiraoka, *J. Chem. Phys.* **89**, 3190 (1988).
[77] G. N. Lewis, *J. Am. Chem. Soc.* **46**, 2027 (1924).
[78] R. Hernandez-Lamoneda and A. Ramirez-Solis, *J. Chem. Phys.* **113**, 4139 (2000).
[79] A. L. Tchougreeff, *Int. J. Quantum Chem* **116**, 137 (2016).
[80] Y. Paukku, Z. Varga, and D. G. Truhlar, *J. Chem. Phys.* **148**, 124314 (2018).
[81] T. K. Mankodi, U. V. Bhandarkar, and B. P. Puranik, *J. Chem. Phys.* **148**, 074305 (2018).
[82] J. Kalcher, *Chem. Phys. Lett.* **403**, 146 (2005).
[83] P. S. Thomas, N. P. Bowling, and R. J. McMahon, *J. Am. Chem. Soc.* **131**, 8649 (2009).
[84] N. P. Bowling, R. J. Halter, J. A. Hodges, R. A. Seburg, P. S. Thomas, C. S. Simmons, J. F. Stanton, and R. J. McMahon, *J. Am. Chem. Soc.* **128**, 3291 (2006).
[85] A. Rauk, *Orbital Interaction Theory of Organic Chemistry* (John Wiley & Sons Inc., New York, NY, 1994).
[86] C. L. Morter, S. K. Farhat, and R. F. Curl, *Chem Phys Lett* **207**, 153 (1993).
[87] R. A. Bernheim, R. J. Kempf, and E. F. Reichenbecher, *J Magetic Resonance* **3**, 5 (1970).

[88] R. A. Bernheim, R. J. Kempf, J. V. Gramas, and P. S. Skell, *J Chem Phys* **43**, 196 (1965).
[89] R. A. Bernheim, R. J. Kempf, P. W. Humer, and P. S. Skell, *J Chem Phys* **41**, 1156 (1964).
[90] E. Wasserman, W. A. Yager, and V. J. Kuck, *Chem Phys Lett* **7**, 409 (1970).
[91] K. S. Kim, H. F. Schaefer III, L. Radom, J. A. Pople, and J. S. Binkley, *J Am Chem Soc* **105**, 4148 (1983).
[92] H. Tomioka, *Acc. Chem. Res.* **30**, 315 (1997).
[93] K. Hirai, T. Itoh, and H. Tomioka, *Chem. Rev.* **109**, 3275 (2009).
[94] J. C. Poutsma, S. D. Upshaw, R. R. Squires, and P. G. Wenthold, *J. Phys. Chem. A* **106**, 1067 (2002).
[95] D. J. Goebbert, K. Pichugin, D. Khuseynov, P. G. Wenthold, and A. Sanov, *J. Chem. Phys.* **132**, 224301 (2010).
[96] D. Khuseynov, M. Fontana, and A. Sanov, *Chem. Phys. Lett.* **550**, 15 (2012).
[97] L. M. Culberson, A. A. Wallace, C. C. Blackstone, D. Khuseynov, and A. Sanov, *Phys. Chem. Chem. Phys.* **16**, 3964 (2014).
[98] A. A. Wallace, Y. Dauletyarov, and A. Sanov, *J. Phys. Chem. A* **125**, 317 (2021).
[99] P. C. Wong, *Can. J. Chem.* **60**, 339 (1982).
[100] I. N. Levine, *Quantum Chemistry* 5th ed. (Prentice-Hall, Inc., Upper Saddle River, NJ, 2000).
[101] E. Hückel, *Z. Phys.* **70**, 204 (1931).
[102] E. Hückel, *Z. Phys.* **72**, 310 (1931).
[103] E. Hückel, *Z. Phys.* **76**, 628 (1932).
[104] E. Hückel, *Z. Phys.* **83**, 632 (1933).
[105] T. Koopmans, *Physica* **1**, 104 (1934).
[106] K. Molcanov, Z. Y. Mou, M. Kertesz, B. Kojic-Prodic, D. Stalke, S. Demeshko, A. Santic, and V. Stilinovic, *Chem-Eur J* **24**, 8292 (2018).
[107] B. Chen, D. A. Hrovat, R. West, S. H. M. Deng, X. B. Wang, and W. T. Borden, *J. Am. Chem. Soc.* **136**, 12345 (2014).
[108] F. L. Hirshfeld, *Theoretica Chimica Acta* **44**, 129 (1977).
[109] P. Bultinck, *Faraday Discuss.* **135**, 347 (2007).
[110] P. Bultinck, C. V. Alsenoy, P. W. Ayers, and R. Carbó-Dorca, *J. Chem. Phys.* **126**, 144111 (2007).
[111] MATLAB, *version R2020a* (The MathWorks, Inc., Natick, Massachusetts, 2020).
[112] T. Sommerfeld, *J. Phys. B* **36**, L127 (2003).
[113] T. Sommerfeld, H. D. Meyer, and L. S. Cederbaum, *Phys. Chem. Chem. Phys.* **6**, 42 (2004).
[114] V. K. Voora, A. Kairalapova, T. Sommerfeld, and K. D. Jordan, *J. Chem. Phys.* **147** (2017).
[115] C. D. Cooper and R. N. Compton, *Chem Phys Lipids* **14**, 29 (1972).
[116] J. Pacansky, U. Wahlgren, and P. S. Bagus, *J. Chem. Phys.* **62**, 2740 (1975).
[117] Y. X. Zhao, C. C. Arnold, and D. M. Neumark, *J. Chem. Soc. Faraday Trans.* **89**, 1449 (1993).
[118] D. W. Arnold, S. E. Bradforth, E. H. Kim, and D. M. Neumark, *J. Chem. Phys.* **102**, 3493 (1995).
[119] D. W. Arnold, S. E. Bradforth, E. H. Kim, and D. M. Neumark, *J. Chem. Phys.* **102**, 3510 (1995).
[120] A. Sanov, J. Faeder, R. Parson, and W. C. Lineberger, *Chem. Phys. Lett.* **313**, 812 (1999).

[121] Y. H. Shao, Z. T. Gan, E. Epifanovsky, A. T. B. Gilbert, M. Wormit, J. Kussmann, A. W. Lange, A. Behn, J. Deng, X. T. Feng, D. Ghosh, M. Goldey, P. R. Horn, L. D. Jacobson, I. Kaliman, R. Z. Khaliullin, T. Kus, A. Landau, J. Liu, E. I. Proynov, Y. M. Rhee, R. M. Richard, M. A. Rohrdanz, R. P. Steele, E. J. Sundstrom, H. L. Woodcock, P. M. Zimmerman, D. Zuev, B. Albrecht, E. Alguire, B. Austin, G. J. O. Beran, Y. A. Bernard, E. Berquist, K. Brandhorst, K. B. Bravaya, S. T. Brown, D. Casanova, C. M. Chang, Y. Q. Chen, S. H. Chien, K. D. Closser, D. L. Crittenden, M. Diedenhofen, R. A. DiStasio, H. Do, A. D. Dutoi, R. G. Edgar, S. Fatehi, L. Fusti-Molnar, A. Ghysels, A. Golubeva-Zadorozhnaya, J. Gomes, M. W. D. Hanson-Heine, P. H. P. Harbach, A. W. Hauser, E. G. Hohenstein, Z. C. Holden, T. C. Jagau, H. J. Ji, B. Kaduk, K. Khistyaev, J. Kim, J. Kim, R. A. King, P. Klunzinger, D. Kosenkov, T. Kowalczyk, C. M. Krauter, K. U. Lao, A. D. Laurent, K. V. Lawler, S. V. Levchenko, C. Y. Lin, F. Liu, E. Livshits, R. C. Lochan, A. Luenser, P. Manohar, S. F. Manzer, S. P. Mao, N. Mardirossian, A. V. Marenich, S. A. Maurer, N. J. Mayhall, E. Neuscamman, C. M. Oana, R. Olivares-Amaya, D. P. O'Neill, J. A. Parkhill, T. M. Perrine, R. Peverati, A. Prociuk, D. R. Rehn, E. Rosta, N. J. Russ, S. M. Sharada, S. Sharma, D. W. Small, A. Sodt, T. Stein, D. Stuck, Y. C. Su, A. J. W. Thom, T. Tsuchimochi, V. Vanovschi, L. Vogt, O. Vydrov, T. Wang, M. A. Watson, J. Wenzel, A. White, C. F. Williams, J. Yang, S. Yeganeh, S. R. Yost, Z. Q. You, I. Y. Zhang, X. Zhang, Y. Zhao, B. R. Brooks, G. K. L. Chan, D. M. Chipman, C. J. Cramer, W. A. Goddard, M. S. Gordon, W. J. Hehre, A. Klamt, H. F. Schaefer, M. W. Schmidt, C. D. Sherrill, D. G. Truhlar, A. Warshel, X. Xu, A. Aspuru-Guzik, R. Baer, A. T. Bell, N. A. Besley, J. D. Chai, A. Dreuw, B. D. Dunietz, T. R. Furlani, S. R. Gwaltney, C. P. Hsu, Y. S. Jung, J. Kong, D. S. Lambrecht, W. Z. Liang, C. Ochsenfeld, V. A. Rassolov, L. V. Slipchenko, J. E. Subotnik, T. Van Voorhis, J. M. Herbert, A. I. Krylov, P. M. W. Gill and M. Head-Gordon, *Mol. Phys.* **113**, 184 (2015).

[122] M. L. Alexander, M. A. Johnson, N. E. Levinger, and W. C. Lineberger, *Phys. Rev. Lett.* **57**, 976 (1986).

[123] T. Nagata, H. Yoshida, and T. Kondow, *Z. Phys. D Atoms Mol. Clusters* **26**, 367 (1993).

[124] Y. Negishi, T. Nagata, and T. Tsukuda, *Chem. Phys. Lett.* **364**, 127 (2002).

[125] A. Muraoka, Y. Inokuchi, N. Nishi, and T. Nagata, *J. Chem. Phys.* **122** (2005).

[126] L. Velarde, T. Habteyes, and A. Sanov, *J. Chem. Phys.* **125**, 114303 (2006).

[127] K. G. Spears, *J. Chem. Phys.* **57**, 1850 (1972).

[128] K. G. Spears and E. E. Ferguson, *J. Chem. Phys.* **59**, 4174 (1973).

[129] B. S. Ault, *Inorg. Chem.* **21**, 756 (1982).